Studies of oxidized hexagonal SiC surfaces and the SiC/SiO_2 interface using photoemission and synchrotron radiation

2004 J. Phys.: Condens. Matter 16 S1783

(http://iopscience.iop.org/0953-8984/16/17/017)

INSTITUTE OF PHYSICS PUBLISHING JOURNAL OF PHYSICS: CONDENSED MATTER

J. Phys.: Condens. Matter **16** (2004) S1783–S1814 PII: S0953-8984(04)65024-7

Studies of oxidized hexagonal SiC surfaces and the SiC/SiO_2 interface using photoemission and synchrotron radiation

C Virojanadara and L I Johansson[1]

Department of Physics and Measurement Technology, Linköping University, S-58183 Linköping, Sweden

E-mail: lij@ifm.liu.se

Received 24 June 2003
Published 16 April 2004
Online at stacks.iop.org/JPhysCM/16/S1783
DOI: 10.1088/0953-8984/16/17/017

Abstract

Results of recent photoemission studies of oxidation of hexagonal SiC surfaces and SiO_2/SiC interfaces are reviewed and discussed. These investigations have focused on two main questions thought to have a significant effect on MOS device characteristics: the existence of carbon clusters or carbon-containing by-products and the existence of sub-oxides at the SiO_2/SiC interface. The presentation is focused on Si-terminated surfaces of hexagonal n-type SiC(0001) crystals since they to date have been considered the most promising for device applications. The results reviewed show that no carbon clusters or carbon-containing by-product can be detected at the interface of *in situ* or *ex situ* grown samples with an oxide layer thickness larger than about 10 Å. Since the presence of carbon clusters was suggested in a recent scanning microscopy study it appears that they may exist, possibly depending on the sample preparation method used, but in such low concentrations that they are not detectable using photoemission. The presence of sub-oxides at the SiO_2/SiC interface has been revealed in recorded Si 2p core level spectra by several groups. The results were not unanimous, however. The number of sub-oxides present and the shifts reported were different. The results of a recent study including also the Si 1s core level and Si KLL Auger transitions are therefore examined. These together with earlier Si 2p data show the presence of only one sub-oxide, assigned to Si^{1+} oxidation states, besides the fully developed SiO_2 (Si^{4+}). Possible reasons for the differences obtained earlier are discussed. That the sub-oxide is located at the interface is concluded from the relative intensity variations observed for the different components versus electron emission angle. An oxide thickness dependence of the SiO_2 chemical shift in the core levels and Auger transitions is shown, similar to but

[1] Author to whom any correspondence should be addressed.

smaller in magnitude than the thickness dependence revealed earlier for SiO_2/Si. On cooled SiC(0001) substrates, adsorption of metastable molecular oxygen is suggested to occur in the initial oxidation stage like on the Si(111)-7 × 7 surface. Oxidation results from the C-terminated SiC(000$\bar{1}$) surface and some preliminary results for the non-polar (10$\bar{1}$0) and (11$\bar{2}$0) surfaces are included and they show distinct differences both as regards the sub-oxides present and the amount of carbon-containing by-products at the interface in the initial oxidation stage compared to the Si-terminated SiC(0001) surface.

1. Introduction

In this paper we try to provide a snapshot of recent progress concerning oxidation of hexagonal SiC surfaces and the SiO_2/SiC interface properties. The scope is limited to results obtained using photoelectron spectroscopy and synchrotron radiation. The presentation is focused on recent results obtained by the authors but these are compared with and discussed in relation to recent findings of other research groups.

A high-quality SiO_2/semiconductor interface with a low defect density is of crucial importance for the performance of metal–oxide–semiconductor (MOS) devices. Since such devices have commonly been fabricated on silicon surfaces, the properties of the SiO_2/Si interface have been intensively studied [1] in the past. Due to the limitations of Si-based devices in high-power, high-temperature, and high-frequency applications, the wide-band-gap semiconductor silicon carbide (SiC) has for some years now been considered a very attractive alternative material for such applications [2]. Since it is the Si-terminated (0001) surface of hexagonal SiC crystals of the 4H and 6H polytypes that have to date been considered the most promising [2–4] for device applications, the presentation is focused on this surface.

The outstanding properties [2, 3] of SiC such as its high breakdown electric field, high saturation electron velocity, and high thermal conductivity give this material a tremendous potential in for example the power device area. Compared to other III–V and II–VI wide-band-gap semiconductors, SiC has also another advantage. An oxide layer can be thermally grown on SiC by heating in an O_2 ambient, exactly like for Si, although the oxidation rate is in general more than an order of magnitude lower. However, the defect densities obtained at SiO_2/SiC interfaces are considerably higher than for SiO_2/Si interfaces, and this is crucial since it actually limits the performance and applicability of SiC-based devices. The formation of carbon clusters and/or carbon-containing by-products at the SiO_2/SiC interface has been suggested [4–6] to be the important factor for the high defect densities. Recent experimental efforts to prove whether carbon or carbon-containing by-products can be detected at the SiO_2/SiC interface are therefore reviewed and discussed in section 3.1. It is shown that no carbon clusters or carbon-containing by-products can be detected at the SiO_2/Si interface of *in situ* or *ex situ* grown samples with an oxide layer thickness larger than about 10 Å. It is moreover shown that surface carbon deliberately created by *in situ* high-temperature anneals can be reduced to below the detection limit by *in situ* oxidation and heating cycles.

The presence of sub-oxides was a major issue for the SiO_2/Si interface. That three sub-oxides (Si^{1+}, Si^{2+}, and Si^{3+}) besides the fully developed SiO_2 (Si^{4+}) can exist at the SiO_2/Si interface is today well known [1]. That sub-oxides inevitably do exist also at the SiO_2/SiC interface was predicted [7] in a recent theoretical calculation. If and what sub-oxides are formed at the SiO_2/SiC interface has therefore attracted considerable attention during the last few years. Recent findings are reviewed and discussed in section 3.2. For the Si-terminated SiC(0001)

surface it is shown that one sub-oxide (Si^{1+}), in addition to the fully developed SiO_2 (Si^{4+}), does exist at the SiO_2/Si interface. Experimental evidence that this sub-oxide is located at the interface is presented. That the core level SiO_2 chemical shifts for SiO_2/SiC samples do exhibit a dependence on the oxide thickness is also shown and compared to earlier findings [1] for SiO_2/Si samples. Experimental evidence that adsorption of metastable molecular oxygen in an *ins-paul* configuration seems to occur in the initial oxidation stage on the SiC(0001)-$\sqrt{3} \times \sqrt{3}$ surface at low temperatures is presented and discussed in section 3.3.

Oxidation results for the C-terminated $(000\bar{1})$ surface and some preliminary findings for the non-polar $(10\bar{1}0)$ and $(11\bar{2}0)$ surfaces of the 4H polytype are presented in section 4. Since these surfaces do contain carbon in the surface layer, they can be expected to show a different behaviour upon initial oxidation compared to the Si-terminated surface. The results presented also show this to be the case. For the C-terminated $(000\bar{1})$ surface a different sub-oxide, tentatively assigned as a Si^{2+} oxidation state, is found to form upon initial oxidation. For the non-polar surfaces, which for ideally bulk truncated crystals should have both Si and C atoms in the surface layer, the presence of two sub-oxides is indicated. Carbon enrichment in the surface region was however observed on these three surfaces. It was moreover found that carbon clusters or carbon by-products at the SiO_2/Si interfaces could be detected even after large oxygen exposures on these surfaces, contrary to the observations made on the Si-terminated surface.

2. Experimental methods and samples

A short introduction to photoemission, and the types of sample and preparation method typically used in the studies of oxidation of SiC surfaces and SiO_2/SiC interfaces is given in this section. For detailed information, readers are referred to the publications referenced in the text.

In photoemission the sample is irradiated by monochromatic radiation and an energy analysis of the emitted photoelectrons and Auger electrons provides information about the chemical species present [1]. Information about the chemical state can also be obtained since the elemental specific core level binding energies exhibit characteristic chemical shifts depending on the chemical surrounding. In studies of SiO_2/SiC samples, one has to be aware of the potential problems with non-conducting materials. Illumination of such samples with intense radiation is likely to induce charging effects that are very difficult to compensate for. A common way to circumvent this problem is to specify only relative binding energies, i.e. the binding energy referenced to a core level of the substrate. In the analysis, one then assumes the same potential in the oxide and substrate which is a reasonable assumption for very thin oxide layers. For thicker layers the shifts determined do contain contributions of different charging and relaxation effects in the oxide and substrate, however. These are the same problems as encountered earlier [1] for SiO_2/Si samples.

The photoemission results presented below have all been collected using synchrotron radiation at different beam lines at MAXlab and HASYLAB. High-resolution studies of Si 2p, Si 1s, and O 1s core levels and of Si KLL Auger transitions are presented and discussed in relation to recent results obtained by other groups. Since the results do not all agree, possible reasons for the differences obtained are discussed.

Hexagonal n-type SiC crystals of the 4H and 6H polytypes, grown along the [0001] direction, have to date been considered the most promising [2–4] for device applications. The 4H polytype has the largest band gap, highest electron mobility, and smallest anisotropy among the many existing SiC polytypes [8]. The (0001) surface of these polytypes is polar, i.e. either Si- or C-terminated. The presentation below is focused on the Si-terminated surface since it

is the one commonly used for device fabrication. In MOS devices oxides thicknesses of one to two thousand ångström are typically used, but by means of photoemission the interface can only be directly studied for considerably thinner oxides layers, typically $\leqslant$50–100 Å. Therefore many of the studies reported to date have been focused on the initial oxide growth after *in situ* oxygen exposures. The preparation of the initial clean surface is then a crucial step. For the Si-terminated SiC(0001) surface two different methods have commonly been applied to prepare clean and well ordered surfaces. An *ex situ* chemical preparation combined with *in situ* heating cycles [9] to produce a $\sqrt{3} \times \sqrt{3}$ reconstructed surface, originating [9, 10] from Si adatoms in T_4 positions on top of the Si-terminated bulk truncated crystal for both 4H and 6H polytypes. The other method combines *in situ* heating and Si deposition cycles to produce a Si-rich 3×3 reconstructed surface, originating [11, 12] from three Si layers on top of the bulk truncated crystal. The effects induced by oxygen exposure of these surfaces at different substrate temperatures have been investigated and these results are compared and discussed.

For making devices, an *ex situ* dry oxidation process in a furnace is commonly used which enables the growth of thick oxide layers. Such *ex situ* grown samples are shown to have a small hydrocarbon contamination on the surface which prevents a very sensitive probing of carbon species at the interface. They are however very useful for investigating the eventual presence of sub-oxides at the interface since they bridge the gap between real MOS interfaces and interfaces produced by *in situ* oxide growth. In the latter case the maximum oxygen partial pressure that can be used is normally limited, so only fairly thin oxide layers, typically less than 20 Å, can be grown.

The C-terminated SiC(000$\bar{1}$) surface prepared by *ex situ* chemical preparation and *in situ* heating cycles shows a 3×3 reconstruction [13] and is carbon enriched. Some results of *in situ* oxidation studies of surface/interface properties for this surface are included and compared to those for the Si-terminated surface. For the non-polar (10$\bar{1}$0) and (11$\bar{2}$0) surfaces no oxidation studies have yet been reported and therefore only some preliminary findings [14] can be included for these.

3. The Si-terminated SiC(0001) surface

3.1. Carbon clusters or carbon by-products at the SiO_2/SiC interface?

Characterizations of oxide layers thermally grown on SiC have been reported, using Auger electron spectroscopy (AES) [15], cross sectional transmission electron microscopy (XTEM) [16], and x-ray photoelectron spectroscopy (XPS) [5]. The XTEM results showed a homogeneous SiO_2 layer with a well defined interface to SiC. The AES results showed that the SiO_2 layer was free from carbon-related compounds except for in the region very close to the SiO_2/SiC interface. The angle-resolved XPS study [5] showed however the presence of quite a large amount of carbon-containing by-products at the SiO_2/SiC interface. This was surprising and initiated further studies.

For this a high photon energy (3.0 keV) was utilized which allowed a direct and simultaneous probing of the SiC substrate, the interface, and the oxide layer, for samples with oxide thicknesses of up to around 50 Å. In the first efforts made [17] the SiO_2/SiC samples were grown using a standard *ex situ* dry oxidation process and they were then kept in a clean container for about a week before doing the measurements. The additional graphite-like C 1s component observed in spectra recorded from these samples was found to originate from carbon on top of the oxide and not at the interface, however. Hydrocarbon contamination during storage was assumed to be the reason and to hinder the detection of carbon that would eventually be at the

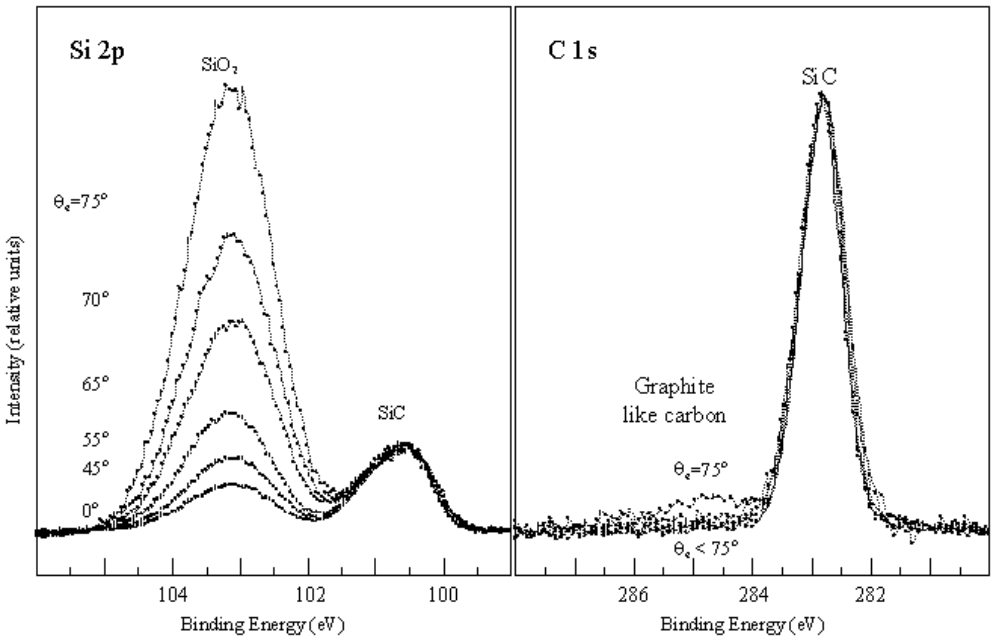

Figure 1. Si 2p and C 1s core level spectra recorded from an *ex situ* grown SiO_2/SiC sample at different electron emission angles using a photon energy of 3 keV.

interface. A different method [18] for minimizing the effects of hydrocarbon contamination was therefore tried. The same *ex situ* oxidation process was applied but thick oxide layers were grown, around 1000 Å thick as measured by a stylus profilometer. The oxide layer was then chemically etched down, using diluted HF and a spinner, just prior to load-locking the samples into the end station for measurements. Si 2p and C 1s core level spectra recorded [18] at different electron emission angles from one of these samples are shown in figure 1. Two peaks are clearly visible in the Si 2p spectrum, one at lower binding energy corresponding to the bulk SiC peak and one at larger binding energy corresponding to SiO_2. In the C 1s spectrum the SiC bulk peak dominates, but at the largest emission angles a weak contribution from a graphite-like C 1s peak located at higher binding energy is also discernible. Both spectra have been normalized to the low-binding-energy peak, so it is only the relative intensities of the two components for various emission angles that are displayed. The relative intensity variation can be utilized to determine from where in the sample the graphite-like carbon signal originates. The intensities of the components in the Si 2p and C 1s spectra were extracted using a curve fit procedure [19]. These values allowed a determination of the intensity ratio between the SiO_2 and the SiC peak for the Si 2p level (labelled Si below) and the ratio between the graphite-like and the SiC peak for the C 1s level (labelled C below) at each emission angle. The ratios obtained are shown in figure 2 and the relative intensity of the Si 2p and C 1s peaks originating from SiO_2 and the graphite-like carbon are seen to increase with increasing emission angle. Applying a simple layer attenuation model, this actually indicates that the graphite-like carbon signal originates from a carbon-containing layer at the surface and not at the interface. The solid curves show the calculated emission angle dependence for an oxide layer thickness of 25.5 Å and a 0.05 Å thick surface graphite-like layer, when electron attenuation lengths [20] of 45 and 50 Å for the C 1s and Si 2p photoelectrons, respectively, are assumed at a photon energy of 3.0 keV. The experimental and calculated intensity variations are seen to agree fairly well.

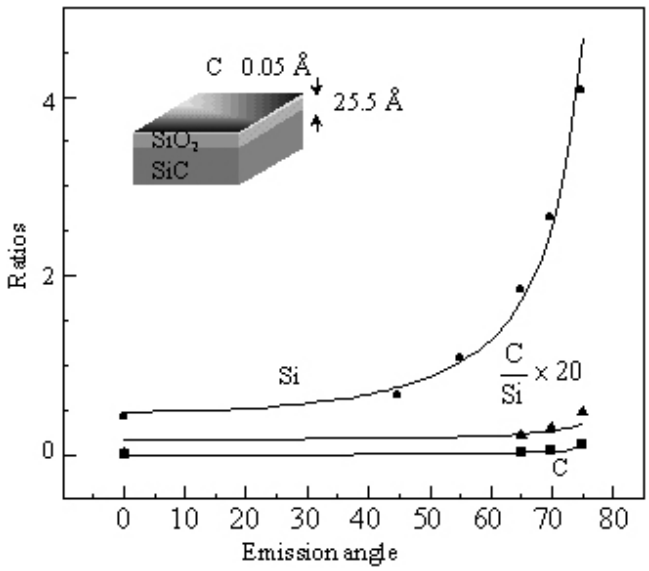

Figure 2. Experimentally extracted intensity ratios C (graphite-like carbon/SiC), Si (SiO_2/SiC), and C/Si (multiplied by 20) for the *ex situ* grown SiO_2/SiC sample are shown by filled squares, circles, and triangles respectively. The solid curves show calculated intensity ratios when assuming the model of the element distribution shown by the inset.

Load-locking the sample immediately after the chemical etching thus considerably reduced the surface carbon contribution but did not completely eliminate it. We could not, however, observe any carbon-containing by-product at the interface. If it existed, the concentration was below the detection limit. The results shown in figures 1 and 2 can be used to estimate the amount required at the interface in order to detect it in these experiments. The graphite-like carbon contribution gave a relative intensity of 0.02 at an emission angle of 65° for this sample. In order to obtain a carbon signal with this relative strength, at an emission angle of 55°, a 0.12 Å thick graphite-like layer at the interface would be required for this sample. If, instead, a compound with an atomic carbon concentration of 0.25 was assumed, corresponding to, for example, $Si_4C_2O_2$, a layer thickness of about 0.5 Å would be required. What could be concluded from these estimates was that if such a carbon-containing layer did exist, it was definitely considerably thinner than the thickness of 8 Å proposed in the earlier investigation [5]. The above results showed that no carbon by-product could be observed at the interface of *ex situ* prepared samples, possibly because of a small but unavoidable hydrocarbon contamination of load-locked samples.

In order to get rid of this surface carbon contamination, *in situ* oxidation experiments were therefore tried [21, 22]. It was found that clean oxide surface/interface/layers could be obtained, where no signal from carbon clusters or carbon by-product at the interface could be detected after oxygen exposures in the 10^6 L range, as illustrated in figure 3. The C 1s spectrum after the oxygen exposure shows only the bulk SiC peak. The C 1s spectrum from the $\sqrt{3} \times \sqrt{3}$ reconstructed surface contains three components. The component labelled S1, at about 0.7 eV lower binding energy than the bulk SiC component, has been interpreted [23, 24] as originating from the uppermost Si–C bilayer of the reconstructed surface. The component labelled S2, at about 1.2 eV higher binding energy than the bulk component, was considered to originate from carbon clusters (graphite-like carbon) on the surface, possibly at steps and

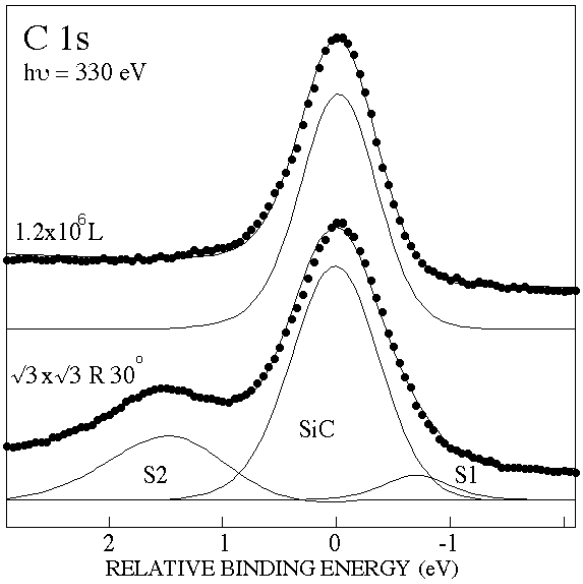

Figure 3. C 1s spectra recorded at $h\nu = 330$ eV before and after oxidation to an exposure of 1.2×10^6 L are shown by the dots. The solid curves through the data points show the result of the curve fit and the curves underneath show the components used; see the text for details.

domain boundaries [10]. It was therefore of interest to monitor how these components were gradually affected by small and up to large oxygen exposures. C 1s spectra recorded from the clean surface and after different oxygen exposures at 800 °C are shown in figure 4. Included in the figure are also two spectra recorded after heating the oxidized sample at 1025 and 1120 °C. After small oxygen exposures the S1 component was found to already decrease quite rapidly and to become undetectable. The S2 component on the other hand did not reduce initially, but in contrast did increase slightly up to an oxygen exposure of 300 L. After an exposure of 10^5 L, however, it was found to be reduced to about half the value obtained on the clean surface, and after an exposure of 1.2×10^6 L it could no longer be detected. The relative intensity extracted for the S2 component is shown in the inset of figure 4. This oxidized sample was then annealed *in situ* for about a minute at 1025 and 1120 °C. The S2 component does not reappear in the C 1s spectrum recorded after these anneals, only the bulk and S1 components. The amount of oxide was found to be strongly reduced after annealing at 1025 °C, and after annealing at 1120 °C no oxide or oxygen signal could be detected. For a clean $\sqrt{3}$ reconstructed SiC surface, such high-temperature anneals normally transform the surface to a mixture of $\sqrt{3}$ and $6\sqrt{3}$ reconstructed domains [23–25]. For such a surface and also for a completely $6\sqrt{3}$ reconstructed surface, the C 1s spectrum is dominated by a broad structure located at a binding energy about 1–2 eV higher than the bulk component [23]. The above results are therefore surprising: that no graphite-like carbon signal could be detected after anneals at such high temperatures and moreover that the sample showed a very clear and intense $\sqrt{3}$ low-energy electron diffraction pattern after the anneal at 1120 °C. We were thus able to prepare a clean and well ordered $\sqrt{3}$ reconstructed surface by first growing an oxide layer on the surface and then removing it by high-temperature annealing. This is further illustrated in figure 5 where C 1s spectra recorded after the three steps are shown. The bottom spectrum shows the initial $\sqrt{3}$ surface prepared by *in situ* heating of an HF-etched and load-locked sample; the middle spectrum, after an

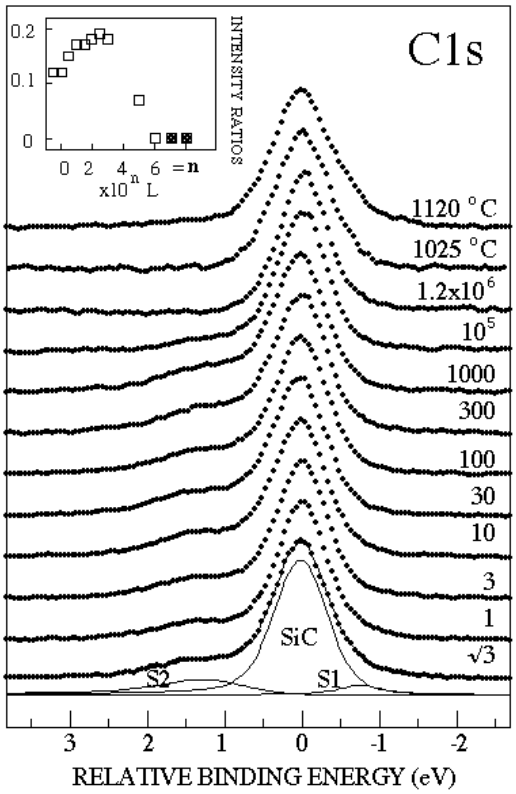

Figure 4. C 1s spectra recorded from SiC(0001), using a photon energy of 330 eV, after different oxygen exposures at 800 °C and also after annealing at two different temperatures after the largest exposure. The inset shows how the relative intensity ratio of the graphite-like carbon (S2/SiC) varies with the oxygen exposure.

oxygen exposure of 1.2×10^6 L at 800 °C; and the top spectrum, after annealing the oxidized sample at 1120 °C for about 1 min. The initial $\sqrt{3}$ surface was prepared at a slightly higher temperature than actually needed for the purpose to obtain a pronounced S2 carbon component on the surface before growing the oxide layer. The C 1s spectra were recorded using a photon energy of 330 eV in order to obtain highest possible surface sensitivity. After oxidation, only the bulk component can be observed. After annealing away the oxide, the surface shifted S1 component originating from the Si–C bilayer of the reconstructed surface reappears but no graphite-like surface carbon component, S2, can be detected.

The results presented above show that no carbon clusters or carbon-containing by-product can be detected at the interface after oxygen exposures in the 10^6 L range, producing oxide layers thicker than about 10 Å. They also show that a very clean $\sqrt{3}$ reconstructed surface can be prepared by *in situ* oxidation and annealing cycles. The former results were also obtained in a recent XPS study [26] where no carbon species could be detected at the interface after thermal oxide growth to a thickness of around 50 Å on both Si-rich 3×3 and C-rich $6\sqrt{3}$ reconstructed surfaces. The results of a recent scanning microscopy study of SiO_2/SiC samples [6] suggested, however, the presence of carbon clusters at the interface, so it appears that they may exist, possibly depending on the sample preparation method used, but in such low concentrations that they are not detectable using photoemission.

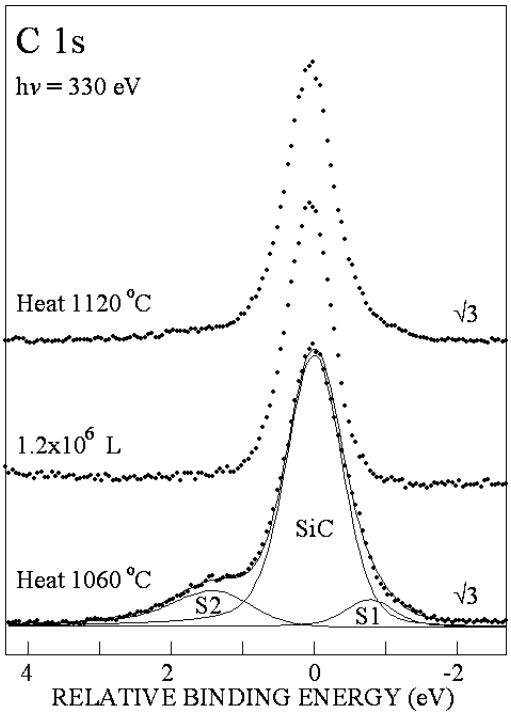

Figure 5. C 1s spectra recorded at $h\nu = 330$ eV from the initial overheated $\sqrt{3} \times \sqrt{3}$ reconstructed surface, after an oxygen exposure of 1.2×10^6 L and after the surface has been regenerated by *in situ* heating; see the text for details.

3.2. Sub-oxides at the SiO_2/SiC interface?

On elemental Si surfaces it is well known [1] that three sub-oxides (Si^{1+}, Si^{2+}, and Si^{3+}) besides the fully developed SiO_2 (Si^{4+}) can form upon oxidation. Photoemission spectra [1, 27] show four shifted Si 2p components which, assuming a formal oxidation state model, correspond to a shift of about 1 eV per nearest-neighbour O atom. For the SiO_2/SiC interface, however, very different results have been reported concerning the number of oxidation states present. In initial oxidation studies of the Si-rich 3×3 reconstructed SiC(0001) surface [28–30], four shifted Si 2p components were reported, i.e. the presence of four Si oxidation states, with energy separations similar to those observed for the oxidized elemental Si surface. The presence of mixed oxides including carbon species (Si–O–C) was also claimed for both the 6H and 4H polytypes and found [30] to be the dominant among the oxide products for the 4H surface. Different results were reported in an XPS study [26] of oxidation of the Si-rich 3×3 and the C-rich $6\sqrt{3} \times 6\sqrt{3}$ reconstructed 6H-SiC surface. After thermal oxide growth to a thickness of around 50 Å no sub-oxides or carbon species could be observed at the interface (within their detection limit) and a shift of 2.5 eV for the SiO_2 (Si^{4+}) component relative to the SiC bulk peak was determined for both surfaces. The results obtained allowed the conclusion to be reached that there is probably no fundamental reason that nearly ideal SiO_2/SiC interfaces cannot be obtained on flat SiC terraces. In a recent angle-resolved study of initial oxidation of the $\sqrt{3} \times \sqrt{3}$ reconstructed 6H-SiC(0001) surface [31], the presence of three additional oxidation states, besides SiO_2, was suggested. Our findings [21, 22, 32] concerning the number of oxidation states present at the interface of SiO_2/SiC samples, thermally grown either *in situ* on

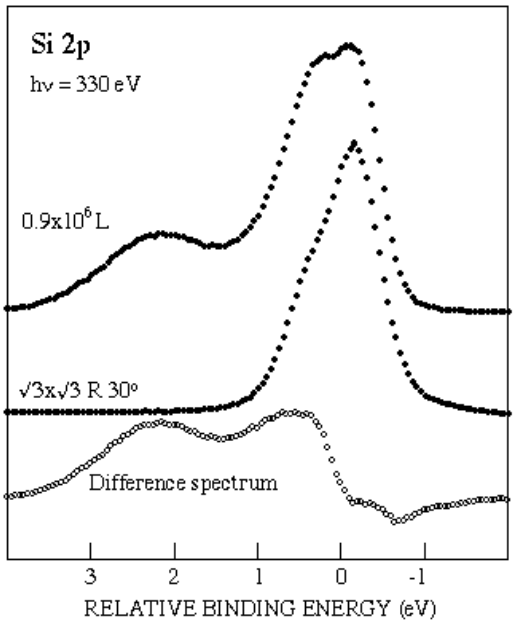

Figure 6. Si 2p spectra recorded at $h\nu = 330$ eV from the clean $\sqrt{3} \times \sqrt{3}$ reconstructed 4H-SiC(0001) surface and after oxidation to a total oxygen exposure of 0.9×10^6 L. The difference spectrum for after and before oxidation is shown by the bottom curve.

$\sqrt{3} \times \sqrt{3}$ reconstructed SiC(0001) surfaces or *ex situ* in a furnace using a standard dry oxidation process, are different. We find that only one sub-oxide can be experimentally verified to exist at these interfaces besides the fully developed SiO_2. In view of these differences in published results, it is worthwhile to review our findings and discuss possible reasons for these differences.

3.2.1. Oxide components observed in Si 2p spectra. Si 2p spectra recorded [21] from the $\sqrt{3} \times \sqrt{3}$ reconstructed 4H-SiC(0001) surface before and after an oxygen exposure of 0.9×10^6 L at a substrate temperature of 600 °C are shown in figure 6. The change in shape of the main Si 2p peak after oxidation indicates the presence of at least one additional Si 2p component located between the SiO_2 (Si^{4+}), and bulk SiC (Si^{0+}) components. The difference spectrum, shown by the bottom curve in figure 6, further illustrates this point. The results of applying a curve fit procedure [19] to Si 2p spectra recorded after this oxidation using photon energies of 130 and 330 eV are shown in figures 7(a) and (b). Since only two additional components are visibly resolved in recorded spectra, only two additional Si 2p components were applied in the fit procedure. This was found to produce fits of good quality and indicated the presence of only one sub-oxide. Since the shift of this additional component was about one fourth of the shift of SiO_2 (Si^{4+}), it was assigned [21] as originating from Si^{1+} oxidation states. The effects of larger exposures and also of somewhat higher substrate temperatures were also investigated. The main effect observed was a larger contribution from SiO_2 while the relative intensity of the Si^{1+} component remained essentially the same, as illustrated in figure 7(c). From these results it was concluded that only one intermediate oxidation state could be experimentally verified after oxygen exposures in the 10^6 L region with the substrate kept at temperatures between 600 and 950 °C. Nothing could be said about initial effects induced after small oxygen exposures and at lower substrate temperatures, so such investigations were therefore a natural next step.

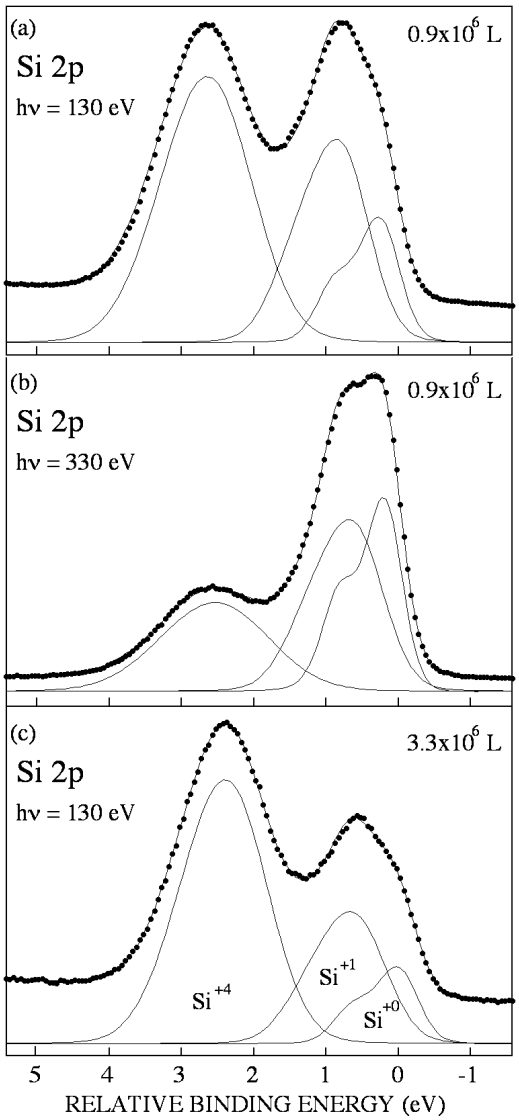

Figure 7. The dots show Si 2p spectra recorded using two different photon energies in (a) and (b) and after two different oxygen exposures in (a) and (c). The solid curves through the data points show the result of the curve fit and the curves underneath show the components used; see the text for details.

The Si 2p spectrum recorded [22] after a 3 L exposure at room temperature (RT) is shown in figure 8 together with fitted curves. Also, this spectrum is composed of three components, the bulk SiC peak and two additional components shifted by ∼0.5 and ∼2.0 eV relative to the bulk peak and corresponding respectively to the Si^{1+} and Si^{4+} oxidation states. The Si^{1+} oxidation state is seen to be considerably stronger than the Si^{4+} state at this low exposure. At larger exposures (30–300 L) the two oxidation states are found to have about the same and fairly constant strength (see below). The development of the oxide components when keeping the sample at 800 °C during exposures is shown in figure 9. The number of additional

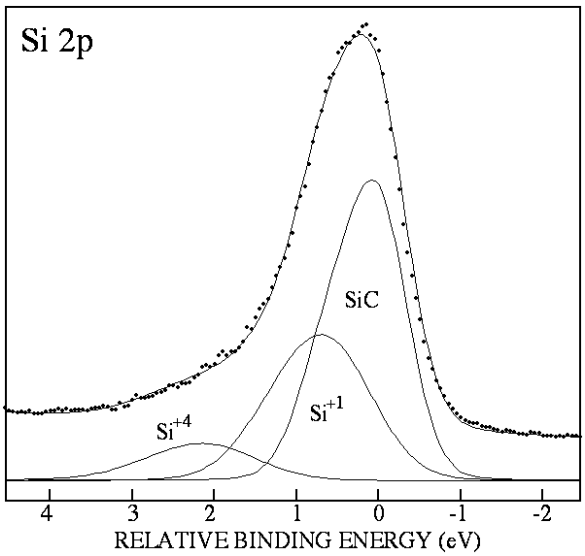

Figure 8. The Si 2p spectrum recorded from SiC(0001)-$\sqrt{3} \times \sqrt{3}$ after an oxygen exposure of 3 L at RT using a photon energy of 130 eV. The solid curve through the data points shows the result of a curve fit and the curves underneath show the components used.

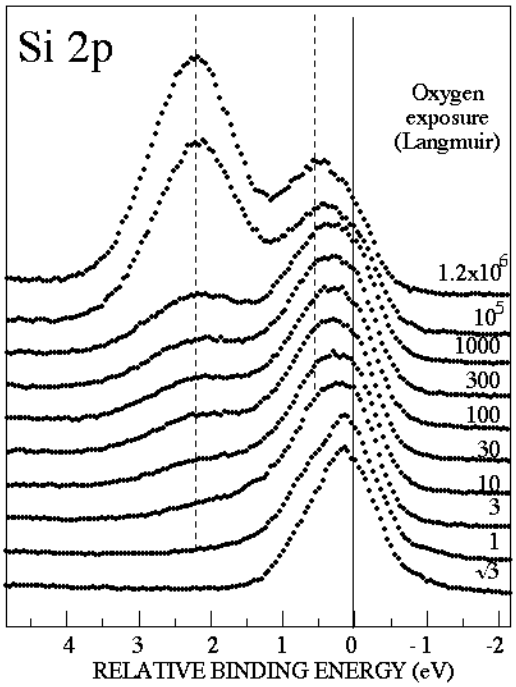

Figure 9. Si 2p spectra recorded from SiC(0001)-$\sqrt{3} \times \sqrt{3}$, using a photon energy of 130 eV, after different oxygen exposures with the sample at 800 °C.

components present and their shifts are found to be the same as at RT. The vertical lines in the figure are guides for the eye and illustrate the locations of the SiC peak and the Si^{1+}

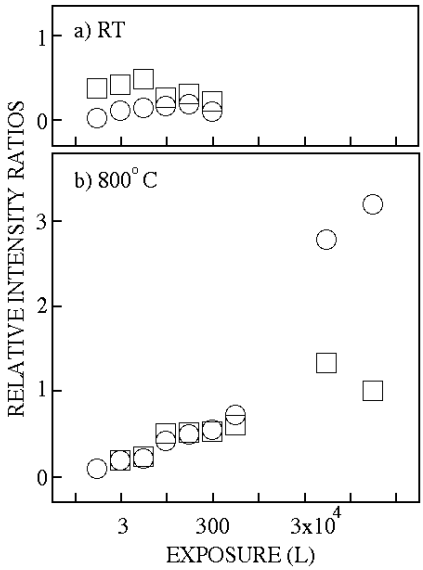

Figure 10. The Si^{1+}/SiC (squares) and Si^{4+}/SiC (circles) intensity ratios extracted from samples oxidized at (a) RT and (b) 800 °C.

and Si^{4+} states. Differences in oxidation rate for the two states are observed, especially at 800 °C. At 1 L exposure no Si^{1+} state and only a very weak Si^{4+} component can be observed. Upon increasing the exposure, the Si^{1+} state becomes visible and both oxide components are seen to increase gradually. At the largest exposures, $\geqslant 10^5$ L, the Si^{4+} component has grown considerably stronger than the Si^{1+} component. The extracted intensity ratios for the Si^{1+} and Si^{4+} components relative to the bulk SiC peak at both 800 °C and RT are shown in figure 10. At RT the Si^{1+} ratio is seen to be fairly constant and larger than the Si^{4+} ratio at all exposures up to 300 L. At 800 °C the ratios for the Si^{1+} and Si^{4+} oxidation states are about equal up to $\leqslant$1000 L but do increase with increasing exposures. At exposures up to $\leqslant$1000 L the oxygen partial pressure was kept below 2×10^{-5} Torr while for the two largest exposures made at 800 °C the oxygen partial pressure was increased to around 10^{-3} Torr. This is most probably the reason that both the oxidation states then increased quite strongly and the Si^{4+} state became dominant. These results that include smaller oxygen exposures and lower substrate temperatures also show that the presence of only one intermediate oxidation state can be experimentally verified.

However, the presence of three additional oxidation states, besides SiO_2, was suggested from the results obtained in an angle-resolved study of initial oxidation of the $\sqrt{3} \times \sqrt{3}$ reconstructed 6H-SiC surface [31]. This was opposite to our earlier findings [21, 22] and therefore we also made some angle-resolved investigations [32] as illustrated in figure 11. There, Si 2p spectra recorded at different electron emission angles from a 4H-SiC(0001) sample exposed to 50 L of oxygen at a substrate temperature of 800 °C are shown. A photon energy of 140 eV was used when collecting these spectra. The dots show the raw data and the solid curve through the data points in the bottom spectrum shows the results from a curve fit procedure using two shifted Si 2p components. The vertical lines indicate the positions of the components that exhibit shifts of 2.1 and 0.5 eV. This is in agreement with earlier findings [21, 22] where the two components were interpreted as originating from Si^{4+} and Si^{1+} oxidation states. This disagrees however with the proposed presence of four oxidation states

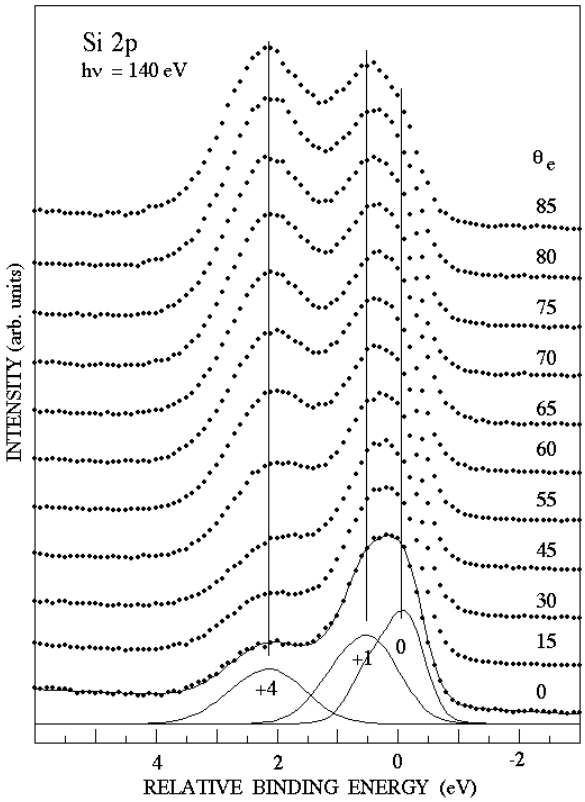

Figure 11. Si 2p spectra from an *in situ* grown SiO_2/SiC sample recorded at different electron emission angles using a photon energy of 140 eV. The dots show the raw data and the solid curve through the data points in the bottom spectrum shows the result from a curve fit procedure using two shifted Si 2p components. The vertical lines indicate the peak positions. See the text for further details.

on the $\sqrt{3} \times \sqrt{3}$ reconstructed 6H-SiC(0001) surface [31]. The Si 2p bulk binding energy is similar for the $\sqrt{3} \times \sqrt{3}$ reconstructed (0001) surface of the 6H and 4H polytypes [23, 33] and the shift determined in [31] for the Si^{4+} oxidation state was only slightly larger compared to the value illustrated in figure 6. The $\sqrt{3} \times \sqrt{3}$ reconstruction originates [9, 10] from Si adatoms on top of a Si-terminated bulk truncated crystal for both 4H and 6H crystals and therefore the different polytypes used cannot explain the suggested difference in oxidation state for these surfaces. In [31] four oxidation states were assumed in the analysis and also equal energy intervals between the Si^{i+} and $Si^{(i+1)+}$ states, although this many components were not visibly resolved in the data collected. We made no such *a priori* assumptions in our analysis [21, 22, 32]. Instead we tried to determine how many shifted components the experimental results indicate to be present and how many are required to adequately model recorded spectra. Despite a good energy resolution in our angle-resolved spectra, only two shifted oxide-related components could be visibly resolved and only two shifted components were required to adequately model recorded spectra. The different results obtained originate thus mainly from the different strategies used in the curve fit procedure applied. The oxide-related structures are fairly wide and overlap quite strongly, so one cannot hope to resolve them in greater detail even if the experimental resolution is further increased. It is therefore

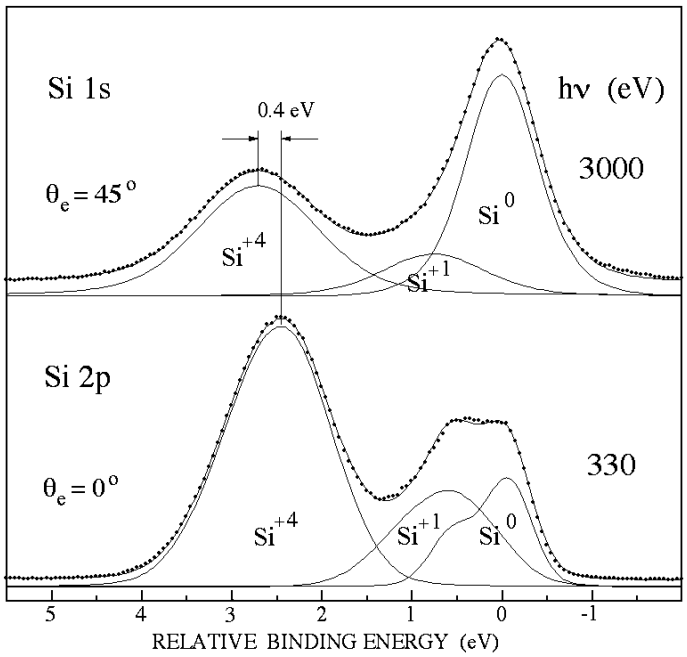

Figure 12. The Si 1s spectrum recorded at an emission angle of 45° using a photon energy of 3.0 keV (upper spectrum) and the Si 2p spectrum from the same sample collected at normal emission using a photon energy of 330 eV (lower spectrum). The solid curves show the fitted results assuming two oxide-related shifted components. A total oxide thickness of 14 Å was determined for this sample.

not meaningful to debate which of the methods used appear most reliable. What appeared more fruitful instead was to investigate whether levels other than the Si 2p one could provide additional information concerning the number of oxidation states present. Studies of the interface on SiO_2/SiC samples with thicker oxides and using higher photon energies were therefore made [32]. Measurements of the Si 1s level and the Si KLL Auger transitions were made for the purpose of obtaining such additional information.

3.2.2. Oxide components observed in Si 1s spectra. A Si 1s spectrum recorded at an emission angle of 45° using a photon energy of 3.0 keV is shown by the upper spectrum in figure 12. The lower one is the Si 2p spectrum collected from the same sample at normal emission using a photon energy of 330 eV. Included in the figure are also curves showing the results fitted using two oxide-related shifted components. The Si 1s spectrum in figure 12 exhibits an asymmetric main peak and one shifted peak originating from SiO_2. The shift of the SiO_2 component is obviously somewhat larger for the Si 1s than for the Si 2p level. The Si 1s spectrum is also simpler to model since it consists of singlets and not of doublets like the Si 2p spectrum. Both of these facts may be advantageous for extracting the different oxidation states despite the larger intrinsic 1s linewidth and the reduced energy resolution at the high photon energies. Angle-resolved studies of the Si 1s level were carried out on SiO_2/SiC samples with oxide thickness values ranging from 7 to 118 Å. How the oxide thickness values were estimated is described in section 3.2.4 below. For the thickest oxide, the SiO_2 component dominated the spectrum. Its line-shape parameters were determined and then used in the fits for the samples with thinner oxides. Clean SiC surfaces, prepared by *in situ* heating of either oxidized samples

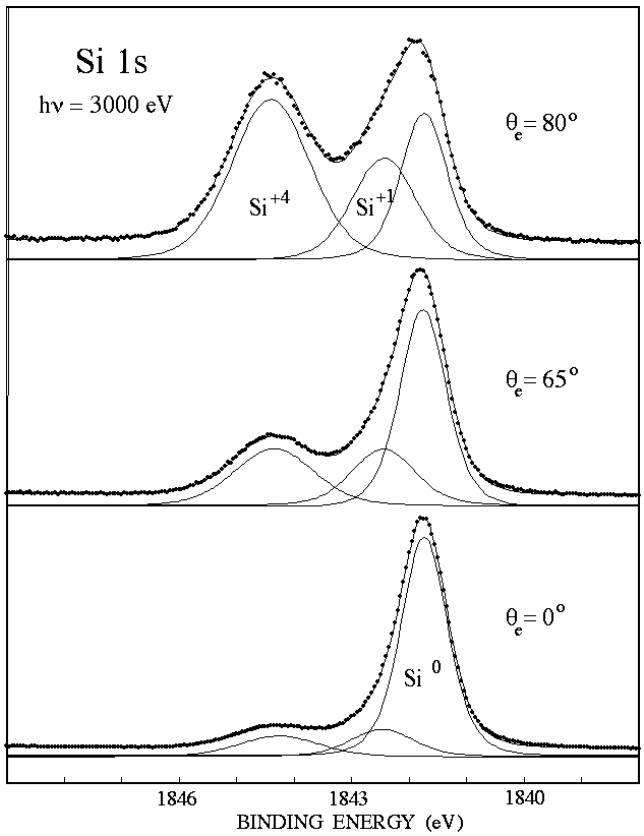

Figure 13. The Si 1s spectrum recorded at three different emission angles and the fitted results.

or HF-etched and load-locked samples, were also investigated. This allowed a determination of the line-shape parameters for the bulk Si 1s peak. The linewidth parameters of the Si^{0+} and the Si^{4+} components determined were then used for all fits of the Si 1s spectra. Only the number of additional components and their widths were varied in the fit procedure. It was found [32] that only one additional shifted component was needed to obtain the best fits to the recorded spectra. This was again interpreted as originating from a Si^{1+} oxidation state since the shift determined for this component was about one quarter of the shift obtained for the Si^{4+} oxidation state. This is further illustrated in figure 13 where Si 1s spectra recorded at three different emission angles from the sample with a 7 Å thick oxide layer are shown. For all samples investigated, similar qualities of the fits were obtained, and we could thus conclude that only two oxide-related shifted components, corresponding to Si^{4+} and Si^{1+} oxidation states, existed on these SiO_2/SiC samples.

3.2.3. Oxide components observed in Si KL $_{2,3}L_{2,3}$ Auger spectra. Whether Si $KL_{2,3}L_{2,3}$ spectra could provide additional information concerning the number of oxidation states present was also investigated [32]. The Si KLL Auger spectra shown in figure 14 were recorded from two different SiO_2/SiC samples at an emission angle of 65°. The total oxide thicknesses were approximately 25 and 10 Å. The Si $KL_{2,3}L_{2,3}$ Auger spectrum from SiC and also from SiO_2 consists of two major peaks (final state multiplet components): a main one at high kinetic

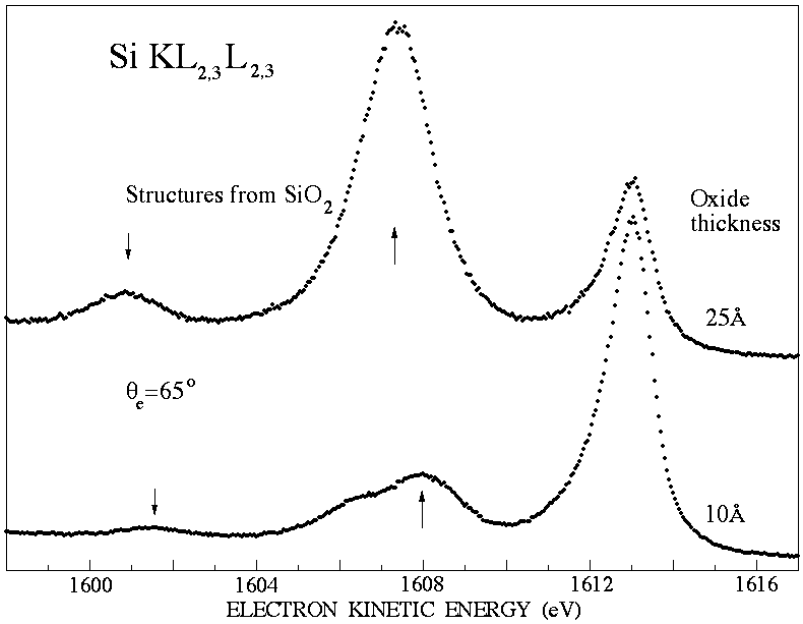

Figure 14. Si $KL_{2,3}$ $L_{2,3}$ Auger spectra from two SiO_2/SiC samples collected at an emission angle of 65°. The total oxide thicknesses were determined as 25 and 10 Å for these samples. The arrows indicate the structures originating from SiO_2.

energy and a considerably weaker one at about 6 eV lower kinetic energy. The locations of the SiO_2 structures are indicated by arrows. These structures completely dominated the Si KLL spectrum recorded from the sample with the thickest oxide (118 Å). A shift of 5.0(±0.1) eV was observed between the main SiC and SiO_2 peaks for the 10 Å oxide sample and a somewhat larger shift, 5.6 eV, for the 25 Å sample. This dependence of the chemical shift on the oxide layer thickness is discussed below in section 3.2.5. The presence of lower oxidation states is not directly discernible in the raw data because of the larger linewidth and overlapping multiplet components. Therefore Si KLL spectra recorded at different electron emission angles from clean SiC and oxidized samples were compared. Si KLL spectra from clean SiC at normal emission (C) and from a sample with a 7 Å thick oxide at emission angles of 0° (Ia) and 75° (Ib) are shown in figure 15. The SiO_2 structures are clearly discernible in the spectra from the oxidized sample and a pronounced asymmetry is also seen on the low-kinetic-energy side of the main SiC peak in the 75° spectrum where the oxide contribution is enhanced. This asymmetry is oxide related since the spectra for clean SiC showed no angle dependence. Since the shape of the KLL multiplet structure is not accurately known, a peak fit analysis alone was not considered sufficient. We therefore also extracted the oxide components from difference curves as illustrated by Ib–Ia and Ib–C in figure 15. They both exhibit, in addition to the two SiO_2-related structures, a pronounced structure around 1612 eV and a weaker one around 1606 eV. These were again interpreted [32] as originating from the presence of a Si^{1+} oxidation state since the main component showed a shift of about one quarter of the shift for the main SiO_2 component. The same result was obtained when analysing in a similar way Si KLL spectra from samples with oxide thickness values of 10, 14, and 25 Å although the relative strength of the Si^{4+} state then became gradually more dominant. These Si KLL results are consistent with the analysis of Si 2p and Si 1s spectra made above which indicated that only a

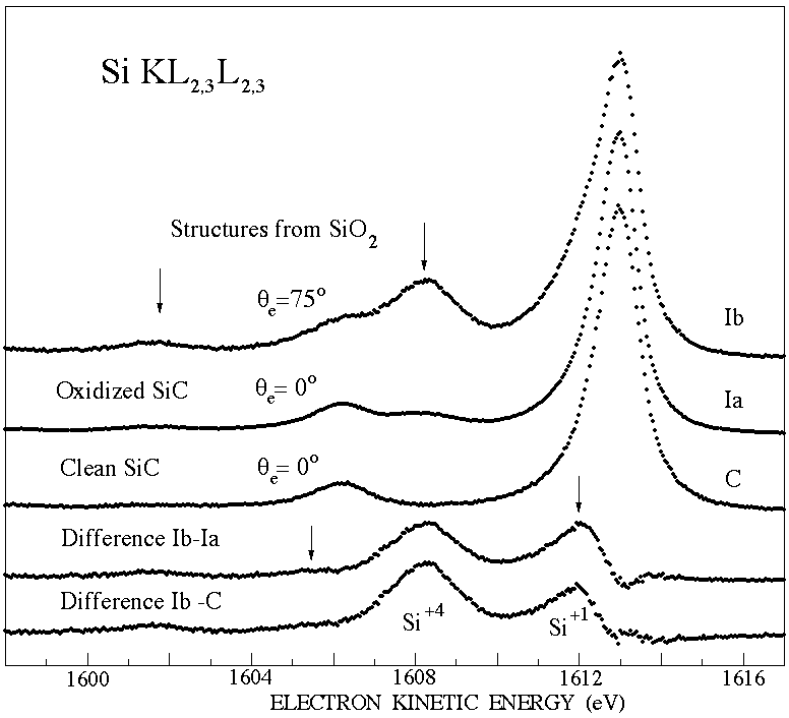

Figure 15. Si $KL_{2,3}$ $L_{2,3}$ spectra from clean SiC at normal emission (C) and from a sample with a 7 Å thick oxide at normal (Ia) and at 75° emission (Ib). The two bottom curves show the Ib–Ia and Ib–C difference curves.

Si^{1+} sub-oxide is present besides Si^{4+} on the SiO_2/SiC samples investigated. The assignment of the additional structures to a Si^{1+} sub-oxide, however, assumes the validity of the formal oxidation state model which has been shown to be justified for core level data.

3.2.4. Location of the sub-oxide? The experimental findings reviewed above show the presence of one sub-oxide on these SiO_2/SiC samples. A simple way to determine whether this sub-oxide forms as a layer at the interface is to analyse the variation in the relative peak intensities versus emission angle within a layer attenuation model. The peak areas of the three different components in the Si 1s spectra were therefore extracted, as illustrated in figure 16. The SiC bulk peak is denoted as Si^0 and the SiO_2 and sub-oxide peaks as +4 and +1, respectively. The SiO_2/SiC (filled circles), sub-oxide/SiC (open squares), and SiO_2/sub-oxide (open circles) peak area ratios were then plotted; see figure 17. Assuming a layer of SiO_2 with a thickness of d_4 on top of a layer of Si_2O sub-oxide with a thickness of d_1, the layer attenuation model predicts the ratios

$$I(4+/\text{bulk}) = \frac{c_{SiO_2}}{c_{SiC}} e^{d_1/(\lambda\cos\theta)}(e^{d_4/(\lambda\cos\theta)} - 1)$$

$$I(1+/\text{bulk}) = \frac{c_{Si_2O}}{c_{SiC}}(e^{d_1/(\lambda\cos\theta)} - 1)$$

where λ is the electron attenuation length and θ is the electron emission angle. When assuming $c_{SiO_2} = 1/3$, $c_{SiC} = 1/2$, and $c_{Si_2O} = 2/3$ (the sub-oxide) to describe approximate values for the atomic concentration ratios, and an electron attenuation length of $\lambda = 23$ Å [20], the

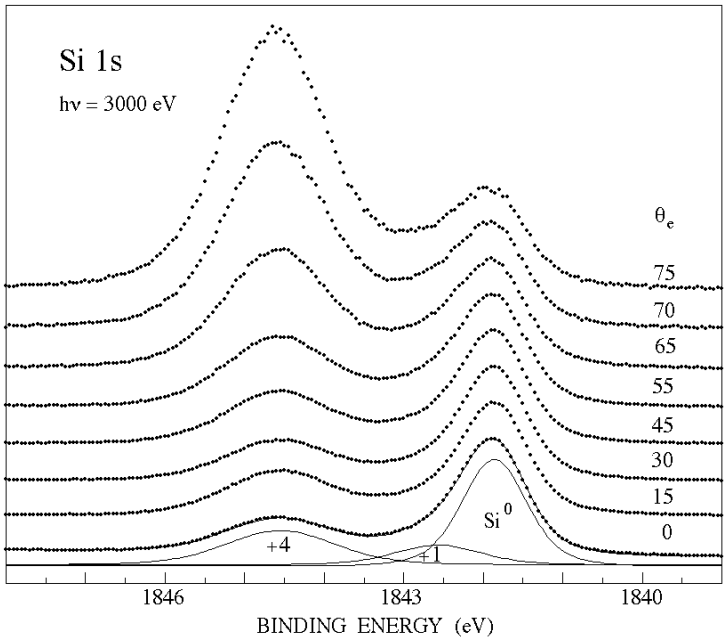

Figure 16. Si 1s spectra collected at different emission angles. The SiC bulk peak is denoted by Si^0 and the SiO_2 and sub-oxide peaks by +4 and +1, respectively.

ratios shown by the solid curves, in figure 17, are obtained for oxide layer thicknesses of $d_4 = 11$ Å and $d_1 = 2.9$ Å. This model for the chemical composition describes well the relative intensity variations observed versus emission angle and shows that the sub-oxide is located at the interface. A total oxide layer thickness of 14 Å was obtained in this case. This modelling was performed also for the samples with total oxide thicknesses of 7, 10, and 25 Å resulting in similarly good agreements between experimental and calculated intensity ratios. The thickness of the sub-oxide varied from 2.5 to 3.5 Å, while the total oxide thickness varied from 7 to 25 Å. For the 118 Å thick oxide, the intensity ratios extracted versus emission angle from Si 2p spectra, recorded using a photon energy of 4.0 keV, were also well described by the above relations, resulting in a sub-oxide thickness of 4 Å. Thus for all samples investigated the relative intensity variations versus electron emission angle were well described by a simple layer attenuation model assuming a Si^{1+} sub-oxide at the interface with a thickness ranging from 2.5 to 4 Å. As regards the thickness values extracted using this simple model, one should be aware of the approximations made and sources of errors [27]. An abrupt interface and the same electron attenuation lengths in the substrate material and the sub-oxide as in SiO_2 were assumed. In addition, the atomic concentration ratios were approximated with values calculated from the chemical formulae and not from the densities of the materials. This latter approximation was estimated to introduce an additional uncertainty of at the most 20% in the values extracted.

3.2.5. The SiO_2 chemical shift. In the Si KLL Auger spectra shown in figure 14 it was noticed that the SiO_2 shift was larger for the 25 Å than for the 10 Å thick oxide. This was also the case for the corresponding shift observed in the Si 1s and 2p core levels. The SiO_2 shifts determined [32] from the curve fits of the core level and Auger spectra are plotted versus

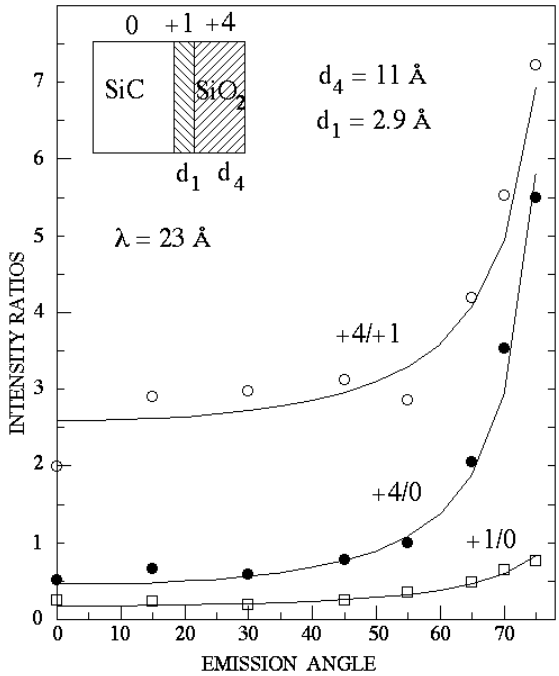

Figure 17. Peak area ratios for SiO_2/SiC (filled circles), sub-oxide/SiC (open squares), and SiO_2/sub-oxide (open circles) extracted versus electron emission angle. The solid curves show the result predicted by the layer attenuation model for oxide layer thicknesses of $d_4 = 11.0$ Å and $d_1 = 2.9$ Å.

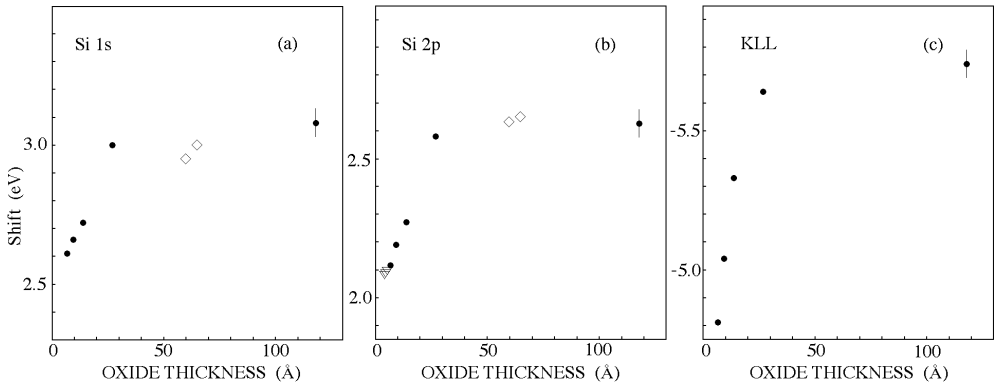

Figure 18. The SiO_2 shift for the (a) Si 1s, (b) Si 2p, and (c) Si $KL_{2,3}$ $L_{2,3}$ lines versus oxide thickness. The uncertainty of ± 0.05 eV in the determination of the shift is shown only for the thickest oxide.

the oxide thickness in figure 18. The circles indicate oxide samples grown to the specified thickness while the open diamonds indicate oxide samples grown as thick as 1000 Å and then etched down prior to measurements using HF. The uncertainty in the determination of the shift was estimated to be ± 0.05 eV so a trend with oxide thickness is clearly visible. The shift increases gradually with increasing oxide thickness up to around 25 Å and remains fairly constant for the thicker oxides. The additional values included in figure 18(b) for the Si 2p

level, and indicated by the open triangles, belong to thinner oxide samples studied using a photon energy of 140 eV (see figure 11). These values, together with earlier findings during initial oxidation [22], indicate that the shift appears to be fairly constant also for oxides thinner than about 10 Å.

This variation of the SiO_2 shift in the Si 2p level with oxide thickness has long been known [1] for SiO_2/Si samples and several suggestions of the cause of it have been given. The presence of different Si–O–Si bond angles (strained SiO_2) near the interface, chemical modifications of the oxide film near the SiO_2/Si interface, a second-nearest-O-neighbour effect, electric charging due to the photon irradiation, and an effect due to electrostatic screening have been proposed. It was argued that all these factors may have an influence on the measured chemical shift but that one has to be aware of charging effects. Also for SiO_2/Si the Si^{4+} shift was found to increase with oxide thickness up to about 25 Å and then to be fairly constant for thicker oxides. The main difference observed was that the overall energy shift with oxide thickness observed for SiO_2/SiC was about a factor of two smaller compared to that for SiO_2/Si. This applied to the Si 2p and 1s core levels as well as to the KLL kinetic energy.

That the KLL energy shift is considerably larger than the core level shifts, see figure 18, indicates a substantial final state relaxation. It is expected, in general, that the Auger shift is more pronounced because—in a classical Coulomb picture—the relaxation contribution for a two-hole final state is four times larger than the corresponding value for a single-hole final state. For SiO_2/Si, an electrostatic image charge potential model was suggested [34] to explain the oxide thickness dependence of the energy shifts. This extra, depth-dependent potential adds to the extra-atomic relaxation energy and qualitatively accounts for the observed shift. Therefore, there seems to be no need to assume additional chemical modifications in the oxide layer for SiO_2/Si. For this system a substantial relaxation contribution has been found [35] and has been attributed to a reduced valence screening in SiO_2. This contribution to the measured SiO_2 chemical shift in the Si 2p level for SiO_2/SiC was quantified utilizing the relative energy shifts displayed in figure 12. An average final state relaxation energy of $\Delta R(2p)$ of about -1.7 eV was determined. For SiO_2/Si a final state relaxation energy of $\Delta R(2p) = -2.1$ eV was recently determined [36] in a similar way for an oxide thickness of around 10 Å.

3.2.6. Possible reasons for the differences. Our core level and Auger data on *in situ* and *ex situ* grown SiO_2/SiC samples revealed the presence of only a Si^{1+} sub-oxide besides SiO_2. That others [31] have suggested that three sub-oxides exist on similarly prepared and oxidized $\sqrt{3} \times \sqrt{3}$ reconstructed SiC(0001) surfaces we propose to be due to the different strategies used in the curve fit procedure applied. In the analysis of recorded Si 2p spectra the authors of [31] assumed four oxidation states with equal energy intervals between the Si^{i+} and $Si^{(i+1)+}$ states to be present, like on elemental Si surfaces, although this many components were not visibly resolved in the data. We had earlier claimed [21, 22] that only one sub-oxide was visibly resolved in Si 2p spectra and that only two oxide components were required to model recorded Si 2p spectra. The Si 1s and Si KLL data [32] presented above show also the presence of only two oxide-related components and thereby support the peak fit procedure that we applied to the Si 2p spectra.

The differences between our results and the oxidation results [26, 28–30] obtained on Si-rich 3×3 reconstructed SiC(0001) surfaces we suggest can be traced to differences in the initial surfaces. The $\sqrt{3} \times \sqrt{3}$ reconstruction is prepared by *in situ* heating and originates [9, 10] from Si adatoms on top of a Si-terminated bulk truncated crystal for both 4H and 6H crystals. The Si-rich 3×3 reconstructed surface is prepared by *in situ* heating and Si deposition, and originates from at least three Si layers [11, 12] on top of the first Si–C bilayer. If one assumes that these surface Si layers are the ones that are initially affected upon oxidation, one expects

the Si-rich 3×3 surface to show properties more like those of an elemental Si surface and also show the same oxidation states. The sub-oxide shifts extracted [29] after small oxygen exposures suggest that this appears to be the case, since they are found to be very similar to the corresponding sub-oxide shifts determined [1, 27] for elemental Si surfaces. After oxygen exposures large enough to oxidize all the surface Si layers and some layers into the SiC substrate, one would expect similar results to be obtained for the 3×3 and $\sqrt{3} \times \sqrt{3}$ surfaces. This also appears to be the case. In the XPS investigation [26] of the 3×3 surface a SiO_2 shift of 2.5 eV relative to the SiC bulk Si 2p peak was reported and this agrees well with our values, shown in figure 18. That this earlier work could not detect any contribution from a Si^{1+} sub-oxide we suggest can be attributed to the lower surface sensitivity and energy resolution that Mg Kα radiation offers compared to synchrotron radiation. There was also reported [26] a shift of -1.2 eV for the Si 2p peak originating from the top Si layers on the clean 3×3 surface relative to the SiC bulk Si 2p peak. This is interesting since it suggests that at intermediate oxygen exposures, when the top Si layers are not completely oxidized, a SiO_2 shift of 3.7 eV would be observed relative to the Si 2p peak from the unaffected Si atoms in these top layers. This we suggest explains the differences observed between the initial oxidation results, obtained using synchrotron radiation, for the Si-rich 3×3 surface [28–30] and the $\sqrt{3} \times \sqrt{3}$ surface [21, 22, 32]. The exposure range investigated for the Si-rich 3×3 surface does not include oxygen exposures large enough to completely oxidize all the top Si layers. The oxide shifts are specified relative to the binding energy of the unaffected Si atoms in these top layers and not to the SiC bulk peak. The SiC bulk Si 2p peak appears to us instead to be assigned [28, 30] to mixed oxide product including carbon species (Si–O–C). This then also explains why such carbon-containing oxide products were claimed to exist on both the 6H and 4H polytypes and to be dominant on 4H surfaces. We could not detect any such carbon-containing oxide products on the $\sqrt{3} \times \sqrt{3}$ reconstructed 4H-SiC(0001) surface. This explanation, however, suggests that it may be possible to prepare a stable Si-rich 3×3 surface that has more Si layers on top of the SiC substrate than the three Si layers [11, 12] determined. This also seems to be the case, as illustrated in figure 19. There Si 2p spectra recorded [37] from a clean Si-rich 3×3 reconstructed surface at two different emission angles using a photon energy of 140 eV are shown by the two lower spectra. This surface showed a very distinct 3×3 LEED pattern and was prepared by *in situ* heating and Si evaporation. A peak decomposition into similar bulk (B) and surface (SS1 and SS2) components as earlier reported [30] is also included in the figure. An interesting observation is that the peak area ratios obtained (SS1/B and (SS1+SS2)/B) are considerably smaller than those reported earlier [29, 30]. The ratios obtained at an emission angle of 30° in figure 19 are a factor of two to three smaller than the ratios obtained in the corresponding 150 eV spectrum reported in [30]. This indicates that the Si-rich 3×3 reconstructed surface can apparently be prepared with different numbers of Si layers on top of the first Si–C bilayer. The effects induced by an oxygen exposure of 1000 L at a substrate temperature of 800 °C are illustrated by the upper spectrum in figure 18. It is clearly seen that the surface Si layers are not completely oxidized even on this 3×3 surface after such an exposure. This observation supports the explanation suggested above for the differences between the results reported for initial oxidation of the 3×3 and $\sqrt{3} \times \sqrt{3}$ surfaces.

3.3. Oxygen adsorption at low temperatures

The initial reaction of O_2 with the $\sqrt{3} \times \sqrt{3}$ reconstructed SiC(0001) surface cooled to liquid nitrogen (LN) temperature has also been studied [38]. Differences between the O 1s peak shape after oxygen exposures with the sample at RT and at an elevated temperature had been noticed, so an even larger effect could possibly be expected for a cooled sample. For the

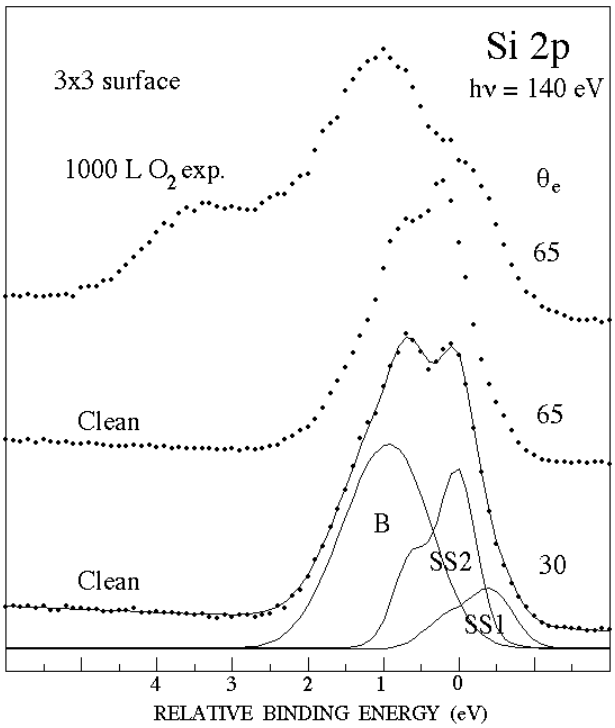

Figure 19. Si 2p spectra from clean 3 × 3 surfaces, prepared by Si evaporation and *in situ* heating, collected at emission angles of 30° and 65° using a photon energy of 140 eV are shown by the two lower spectra. Components fitted to the 30° spectrum are also shown by the solid curves. The upper spectrum was recorded at an emission angle of 65° after an oxygen exposure of 1000 L.

Si(111)-7 × 7 surfaces, initial adsorption of metastable oxygen had been reported [39] and the SiC(0001)-$\sqrt{3} \times \sqrt{3}$ surface has structural similarities with the Si(111)-7 × 7 surface since it also has Si adatoms in the top layer. O 1s spectra recorded after a 1 L oxygen exposure with the sample kept at LN temperature, at RT, and at 800 °C are shown in figure 20. The 800 °C spectrum is seen to contain a main O 1s peak while the other two spectra exhibit an additional structure at lower binding energy and a considerably broader main peak. These differences are illustrated in more detail by the bottom curve, which is a difference spectrum for the LN and 800 °C spectra. The 800 °C spectrum shows the O 1s line shape obtained when growing a stable oxide layer on SiC(0001). At this temperature no significant changes in the O 1s line shape could be observed on increasing the exposure from 1 up to 1.2×10^6 L, producing an oxide layer more than 10 Å thick for which the Si^{4+} oxidation state dominated [21, 22]. Separate contributions from Si^{4+} and Si^{1+} oxidation states can be identified in recorded Si 2p spectra [21, 22] but not in recorded O 1s spectra. The O 1s spectrum always appears as one slightly asymmetric peak and when applying a curve fit procedure two components were therefore used: a main one (labelled O1 below) at about 531.9 eV binding energy and a weaker one (O2) around 533.0 eV. These two components thus merely reflect the asymmetry in the O 1s peak shape and are not associated with different oxidation states. The difference spectrum and the LN and RT spectra indicate that the latter two are likely to contain three additional components. The relative intensity of these components is seen to be strongest in the LN spectrum but they are also present in the RT spectrum.

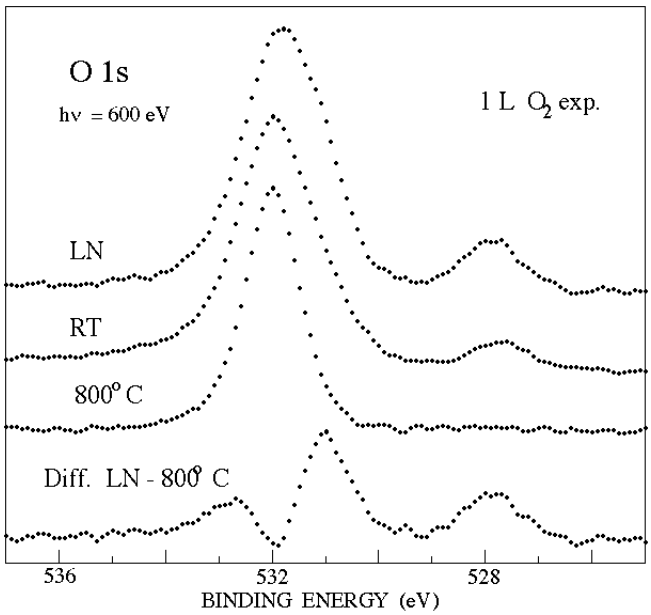

Figure 20. O 1s spectra recorded after a 1 L exposure with the SiC sample kept at three different temperatures. The bottom curve shows a difference spectrum.

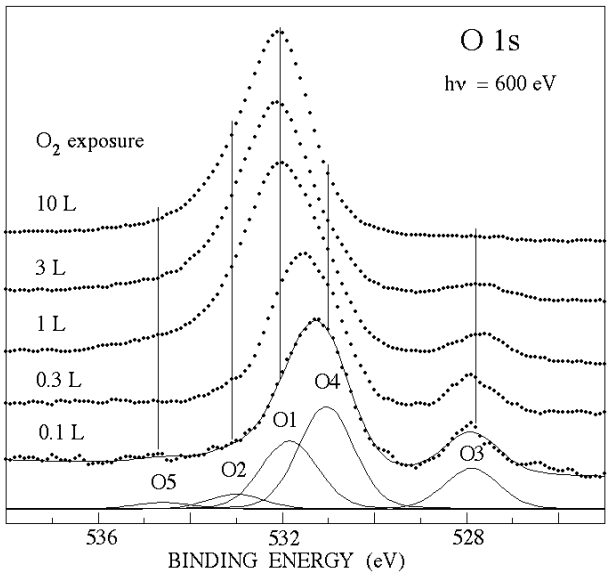

Figure 21. O 1s spectra recorded after different exposures at LN temperature. The bottom curves show the fitted components.

A set of O 1s spectra recorded after different oxygen exposures at LN temperature are shown in figure 21. The five components used in the fit procedure are labelled O1–O5 and shown by the bottom curves in the figure. The vertical dashed lines are guides for the eye displaying their locations. Binding energies of 532.0, 533.1, 531.0, 527.8, and 534.7 eV were extracted for respectively the O1, 2, 3, 4, and 5 components. The O3 and O4 components are

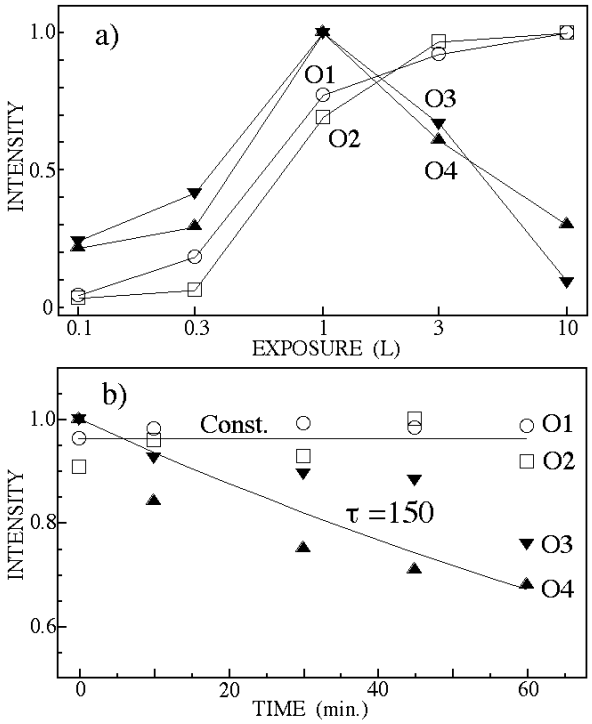

Figure 22. Variation of the extracted peak areas; (a) versus exposure and (b) versus time after the exposure. The peak area (intensity) of each component has been normalized with its maximum value.

seen to give large contributions only at the smallest exposures, while the contributions from the O1 and O2 components are seen to increase with increasing exposure and dominate completely at the largest exposure. At exposures larger than 10 L only the O1 and O2 components are essentially detectable. How the extracted peak areas varied with the exposure is illustrated in figure 22(a). The O5 component was omitted from this figure since it was so weak that its intensity could not be extracted with enough reliability. It was however used in the fit procedure since it improved the quality of the fits and since a similar component was observed [40] in the O 1s spectrum after oxygen exposures on the Si(111)-7 × 7 surface.

The time evolution of the different components was also investigated. In figure 22(b) it is shown how the extracted peak areas varied during one hour after an exposure of 1 L at LN temperature. The O1 and O2 components were found to remain essentially constant and were actually the only ones observable after oxygen exposures made at 800 °C or after large exposures at RT and LN temperature. These components were therefore associated with the formation of stable oxides. The other components did decay with time and were therefore associated with metastable oxygen. A curve showing the decay rate ($y = \exp(-t/\tau)$) assuming a lifetime (τ) of 150 min for the metastable oxygen is included in the figure. This value represented a rough estimate of the lifetime only, since the decay was not monitored for long enough to allow a careful determination. However, the results showed the presence of metastable oxygen after oxygen exposures in the range 0.1–10 L at LN temperature.

On the Si(111)-7 × 7 surface the presence of metastable oxygen had earlier been shown in the initial oxidation stage [39]. There was lively debate on whether this metastable oxygen was molecular or atomic, but recent results [40] suggested metastable molecular oxygen. This

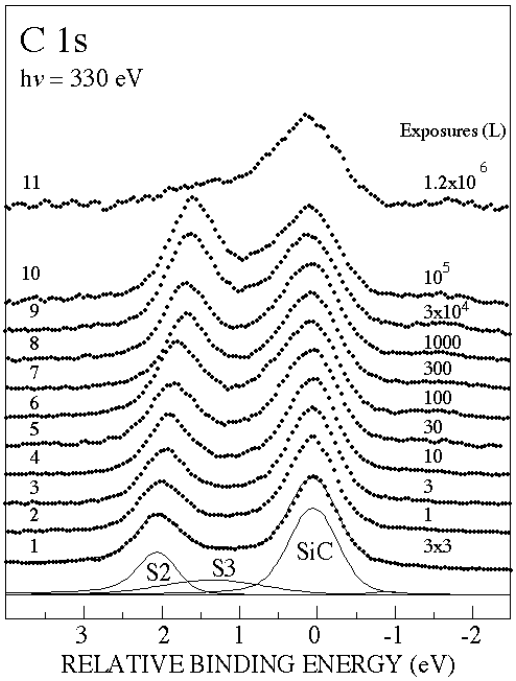

Figure 23. C 1s spectra recorded from SiC(000$\bar{1}$) after different oxygen exposures at 800 °C, using a photon energy of 330 eV. The labels 1–11 denote exposures from 0 to 1.2×10^6 L, as in figure 24.

was suggested since three metastable oxygen components were revealed in the O 1s spectrum and earlier findings had indicated [39, 41] that molecular oxygen configurations with at least three oxygen atoms with different chemical environments had to be considered. It had been suggested [39, 41] that metastable molecular species adsorb on Si adatoms which have at least one back bond modified by an oxygen atom. The O 1s spectrum on the Si(111)-7 × 7 surface [40] showed three metastable components with very similar energy locations to the O3, O4, and O5 components observed in this case. Calculated O 1s binding energies for different oxygen adsorption configurations were presented [40] and they showed that this number of metastable components and their energy separations in the O 1s spectrum could only be accounted for by molecular species in an *ins-paul* adsorption configuration. Since the experimental observations in the two cases are very similar, this suggests that adsorption of metastable molecular oxygen in an *ins-paul* configuration may occur also in the initial oxidation stage on the SiC(0001)-$\sqrt{3} \times \sqrt{3}$ surface.

4. Other SiC surfaces

4.1. The C-terminated (000$\bar{1}$) *surface*

C 1s spectra recorded [22] from the 3 × 3 reconstructed C-terminated (000$\bar{1}$) surface before and after different oxygen exposures at 800 °C are shown in figure 23. Two dominant features are clearly resolved in the spectrum. However, when applying a curve fit procedure, three components have to be used to obtain a reasonable fit, as illustrated by the bottom curves. The need to use three components for this surface had been pointed out earlier [42] and suggested to

indicate that the reconstruction does not originate from a 3×3 arrangement of carbon adatoms on top of a bulk truncated SiC surface, but instead from at least two different carbon layers. The S2 component, shifted by ∼1.7 to higher binding energy, was assigned [42] to carbon sites in a top layer while the S3 component, shifted by ∼0.6 eV to higher binding energy, was assigned to a carbon layer underneath, containing inequivalent carbon sites that give rise to this broad feature. Both the location and the relative intensity of the S2 component are seen to be affected by oxygen exposure. The extracted S2/bulk intensity ratio showed a monotonic increase in strength up to an exposure of 10^5 L. However, after an exposure of 1.2×10^6 L the relative intensity decreased dramatically, down to less than 50% of the value obtained for the initial 3×3 surface. The increase in the ratios was first thought to be due to carbon surface segregation [24] since the sample was kept at 800 °C during the exposures. However, exposures made at RT showed a similar effect so this cannot be the reason. Since a small amount of CO and other carbon-containing molecules is always present in a vacuum system, a slight increase of cracked carbon on the surface with time can be expected, especially after heating. The large increase observed on C-terminated surfaces was however puzzling and could not be explained. That the ratio decreased dramatically after the largest exposure was interpreted as being due to the oxygen then being able to 'burn off' surface carbon since the oxygen partial pressure was higher during that large exposure. The energy separation between the S2 and bulk SiC component is, in figure 23, seen to decrease with exposure, an effect that was not observed for the graphite-like carbon component on the Si-terminated surface. This was interpreted [23] as indicating that the surface carbon layers on 3×3 reconstructed SiC$(000\bar{1})$ were affected and involved in the initial oxidation process.

Si 2p spectra recorded [23] from the 3×3 reconstructed C-terminated $(000\bar{1})$ surface before and after different oxygen exposures at 800 °C are shown in figure 24. The exposures, labelled 1–11, are the same as those specified in figure 23. Compared to the results obtained for the Si-terminated surface (shown in figure 9 above), there are some distinct differences. No Si^{1+} oxidation state can be detected on this surface. Instead a component having a shift of about 1.5 eV is clearly resolved at the intermediate exposures. The Si^{4+} oxidation state, which becomes the dominant feature at the largest exposures, shows a somewhat larger shift on this C-terminated surface. For the Si-terminated surface the Si^{4+} component could already be detected after an exposure of 1 L, while for the C-terminated surface it was not observable until after an exposure of 1000 L (the curve labelled 8 in figure 24). The energy separations extracted after the different exposures are shown in the inset of figure 24. The peak decomposition obtained for the Si 2p spectrum, recorded using a photon energy of 330 eV, after an exposure of 10^5 L is shown in figure 25. The component exhibiting the largest shift, ∼2.7 eV, was assigned to the Si^{4+} oxidation state while the component having a shift of ∼1.5 eV was tentatively assigned to Si^{2+} oxidation states, since the shift was about half of that for the Si^{4+} component. Only this Si^{2+} oxidation state could be detected after oxygen exposures of up to 1000 L made at RT.

That a different sub-oxide component was observed on the C-terminated surface as compared to the Si-terminated surface was attributed to the presence of carbon at the surface and interface. The C 1s spectra, in figure 23 above, showed that the surface- and interface-related carbon components could not be eliminated even after the largest exposures, and at smaller exposures they were found to shift in energy and increase in relative strength. Therefore the Si^{2+} oxidation state observed on the C-terminated surface was assigned as originating from a mixture of Si–C–O bondings. This could then also explain why on this surface the Si^{2+} component was the dominant one at small exposures and why the Si^{4+} component was not detected until after an exposure of 1000 L, while on the Si-terminated surface it was detectable after an exposure of 1 L.

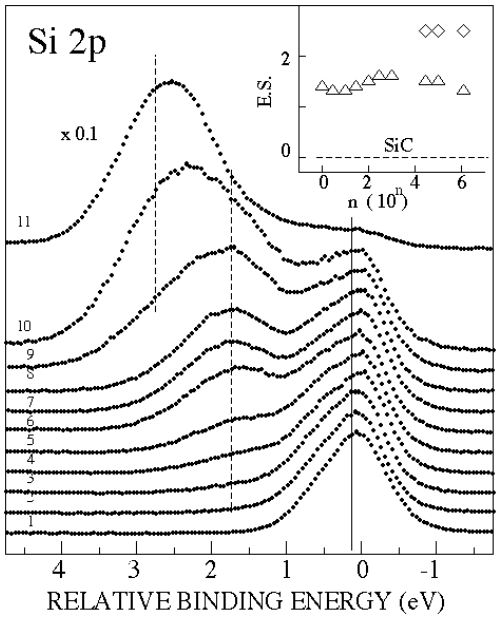

Figure 24. Si 2p spectra recorded from SiC(000$\bar{1}$) after different oxygen exposures at 800 °C, using a photon energy of 130 eV. The different exposures are labelled 1–11, as in figure 23. The inset shows the energy separation (E.S.) extracted for the Si^{2+} (triangles) and Si^{4+} (diamonds) components relative to the bulk SiC component after the different exposures.

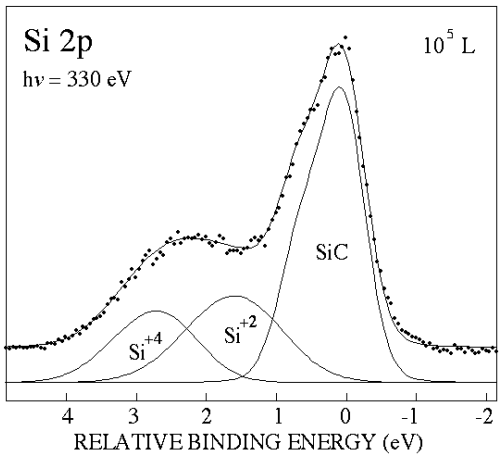

Figure 25. The Si 2p spectrum recorded from SiC(000$\bar{1}$), using a photon energy of 330 eV, after an oxygen exposure of 10^5 L at 800 °C. The solid curve through the data points shows the result of a curve fit and the curves underneath show the components used.

Also, for the oxidized C-terminated surfaces, efforts were made to recreate a 3×3 reconstructed surface with a lower surface carbon content than that initially obtained by heating away the oxide *in situ*, since that had been found to work surprisingly well for oxidized Si-terminated surfaces. This was found not to work for C-terminated surfaces, however. On heating to a high enough temperature for the oxide to start to decompose, a rapid increase in the surface-related C 1s components was always observed.

4.2. Non-polar surfaces

The non-polar $(10\bar{1}0)$ and $(11\bar{2}0)$ surfaces have received considerable recent interest [43, 44] for device applications. It has been proposed [45] that these surfaces, unlike the polar surfaces, can be completely passivated by a single SiO_2 adlayer. No detailed photoemission studies of these surfaces or of the effects induced upon initial oxidation have yet been published, however. Therefore only some preliminary results [14] for these surfaces can be included, that suggest that sub-oxides do exist also on these surfaces and that the number of oxidation states seems to be different to that for the polar surfaces. Si 2p spectra recorded at normal emission (bulk sensitive) and at an emission angle of 70° (surface sensitive) from the two non-polar surfaces after an oxygen exposure of 1000 L at a substrate temperature of 800 °C are shown in figures 26(a) and (b). For comparison, similar spectra recorded from the polar (0001) surface are shown in figure 26(c). Curves fitted to the 70° spectra are also included in the figure. These show that two sub-oxides besides a SiO_2 component appear to form on the non-polar surfaces. The shifts of the SiO_2 component were found to be slightly different, by about 0.2 eV, for the two surfaces, but fairly similar to the values observed for the Si- and C-terminated surfaces. The two sub-oxides were found to have chemical shifts of about 0.5 and 1.5 eV and are therefore assigned as Si^{1+} and Si^{2+} oxidation states. The Si^{2+} sub-oxide is again tentatively suggested to originate from C–Si–O bonding. These non-polar surfaces have both Si and C atoms in the surface layer for bulk truncated crystals [45]. Carbon enrichment in the surface region was however observed [14] on the clean surface prepared by *in situ* heating. It was also found that a weak signal from graphite-like carbon could be detected at the SiO_2/Si interfaces after oxygen exposures in the 10^6 L region, like on the C-terminated surface, although less intense. This is illustrated in figure 27 where C 1s spectra recorded, using a photon energy of 330 eV, from the $(11\bar{2}0)$, $(10\bar{1}0)$, and $(000\bar{1})$ surfaces after an oxygen exposure of 10^6 L are shown.

5. Summary and conclusions

The existence of carbon clusters or carbon-containing by-products and the existence of sub-oxides at the SiO_2/SiC interface are two points thought to have a significant effect on MOS device characteristics. Photoemission studies reported of oxidation of hexagonal SiC surfaces and SiO_2/SiC interfaces have therefore mainly focused on these issues. Recent progress concerning such characterizations has been reviewed, and concentrated on Si-terminated surfaces of hexagonal n-type SiC(0001) crystals, since they have to date been considered the most promising for device applications.

The results presented for *ex situ* and *in situ* grown SiO_2/SiC samples [17, 18, 21, 22, 26] show that no carbon clusters or carbon-containing by-product can be detected at the interface of such samples with an oxide layer thickness larger than about 10 Å. For thinner oxide layers, i.e. after small oxygen exposures with the substrate at RT or heated to temperatures up to 800–900 °C, the presence of carbon-containing by-products could be detected [22, 30] at the interface, however. It was shown that these carbon by-products could be eliminated [22, 26] by larger oxygen exposures, and it was also shown [22] that a clean and well ordered SiC(0001)-$\sqrt{3} \times \sqrt{3}$ surface could be re-created by *in situ* heating of the oxidized sample. However, since the presence of carbon clusters was suggested in a recent scanning microscopy study [6], it appears that they may exist, possibly depending on the sample preparation method used, but in such low concentrations that they are not detectable using photoemission.

The presence of sub-oxides at the SiO_2/SiC interface has been revealed in recorded Si 2p core level spectra by several groups [21, 22, 28–32]. These results were not unanimous, however. The number of sub-oxides present and the shifts reported were different. Therefore

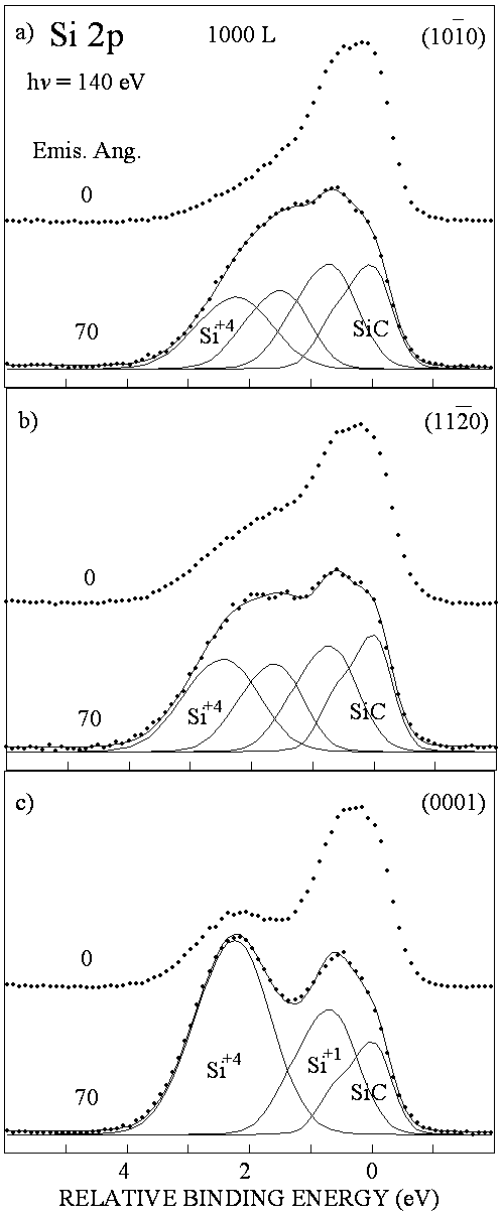

Figure 26. Si 2p spectra recorded from the (a) (10$\bar{1}$0), (b) (11$\bar{2}$0), and (c) (0001) surfaces of SiC after an oxygen exposure of 1000 L. The spectra were collected at two different emission angles, 0° and 70°, using a photon energy of 140 eV. Fitted components are also shown.

the results of a recent angle-resolved study [32] including also the Si 1s core level and Si KLL Auger transitions were presented in some detail. These together with earlier Si 2p data showed the presence of only one sub-oxide, assigned to Si^{1+} oxidation states, besides the fully developed SiO_2 (Si^{4+}). The differences in earlier results reported were suggested to originate from differences in the initial surface investigated [28–30] or to a different strategy used in the curve fit procedure applied in the analysis of the recorded Si 2p spectra [31]. That the sub-oxide

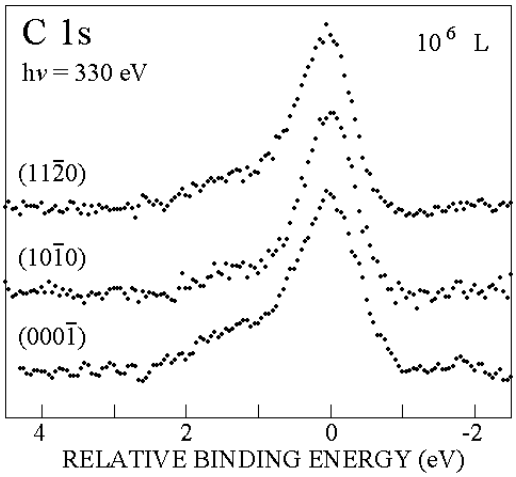

Figure 27. C 1s spectra recorded after an oxygen exposure of 10^6 L at $h\nu = 330$ eV from the (000$\bar{1}$), (10$\bar{1}$0), and (11$\bar{2}$0) surfaces of SiC.

was located at the interface could be concluded from a comparison of oxide/SiC peak intensity ratios extracted versus electron emission angle with the variation predicted using a simple layer attenuation model. The SiO_2 chemical shift was shown to exhibit a characteristic oxide thickness dependence in both the core levels and Auger transitions [32]. This dependence was found to be similar, but smaller in magnitude, as compared to the thickness dependence revealed earlier for SiO_2/Si samples [1]. Possible explanations [1] for this dependence have been given earlier. The KLL energy shift was shown to be considerably larger than for the core level shifts, which indicated a substantial final state relaxation. This contribution to the SiO_2 chemical shift in the Si 2p level for SiO_2/SiC could be quantified by utilizing the relative energy shifts determined for the Si 2p, Si 1s core levels and the Si KLL Auger transitions.

For SiC(0001) samples oxidized *in situ* at RT or at higher temperatures, the O 1s spectrum always appeared as one slightly asymmetric peak. Thus separate contributions from Si^{4+} and Si^{1+} oxidation states could not be identified as in recorded Si 2p spectra [21, 22, 32]. O 1s spectra recorded after small oxygen exposures with the sample kept at LN temperature showed [38] however the presence of five components. The relative intensity of these components versus exposure and with time showed that three of these were associated with metastable oxygen. Adsorption of metastable molecular oxygen in an *ins-paul* configuration was suggested to occur in the initial oxidation stage like on the Si(111)-7 × 7 surface [40].

Oxidation results from the C-terminated SiC(000$\bar{1}$) surface [22] and some preliminary results for the non-polar (10$\bar{1}$0) and (11$\bar{2}$0) surfaces [14] have also been included. They showed distinct differences as regards both the sub-oxides present and the amount of carbon-containing by-products at the interface in the initial oxidation stage compared to the Si-terminated SiC(0001) surface. These differences were attributed to the presence of surface and interface carbon that was found not to be completely eliminable even with the largest oxygen exposures investigated. The presence of a sub-oxide, tentatively assigned as a Si^{2+} oxidation state, could be observed and was proposed to originate from a mixture of Si–C–O bondings. Since very few experimental studies of oxidation and SiO_2/SiC interface properties of these surfaces have been published to date, although the non-polar surfaces have become of recent interest for device applications, they will certainly receive considerably more attention in the years to come.

Acknowledgments

The authors gratefully acknowledge the support from SiCEP and the Swedish Research Council and the fruitful cooperation with our co-authors in earlier publications.

References

[1] Iwata S and Ishizaka A 1996 *J. Appl. Phys.* **79** 6653 and references therein
[2] Morkoc H, Srite S, Gao G B, Lin M E, Sverdlov B and Burns M 1994 *J. Appl. Phys.* **76** 1363
[3] Afanasev V V, Bassler M, Pensel G and Schultz M J 1997 *Phys. Status Solidi* a **162** 321
[4] Li H F, Dimitrijev S, Sweatman D, Harrison H B, Tanner P and Feil B 1999 *J. Appl. Phys.* **86** 4316
[5] Hornetz B, Michel H-J and Halbritter J 1994 *J. Mater. Res.* **9** 3088
[6] Chang K C, Nuhfer N T, Porter L M and Wahab Q 2000 *Appl. Phys. Lett.* **77** 2186
[7] Buczko R, Pennycook S J and Pantelides S 2000 *Phys. Rev. Lett.* **84** 943
[8] Yano H, Hirao T, Kimoto T and Matsunami H 2001 *Appl. Phys. Lett.* **78** 374
[9] Owman F and Mårtensson P M 1995 *Surf. Sci.* **330** L639
[10] Coati A, Sauvage-Simkin M, Garreau Y, Pinchaux R, Argunova T and Aid K 1999 *Phys. Rev.* B **59** 12224
[11] Starke U, Schardt J, Bernhardt J, Franke M, Reuter K, Wedler H, Heinz K, Furthmüller J, Käckel P and Bechstedt F 1998 *Phys. Rev. Lett.* **80** 758
[12] Reuter K, Bernhardt J, Wedler H, Schardt J, Starke U and Heinz K 1997 *Phys. Rev. Lett.* **79** 4818
[13] Nakanishi S, Tokutaka H, Nishimori K, Kishida S and Ishihara N 1989 *Appl. Surf. Sci.* **41/42** 44
[14] Virojanadara C and Johansson L I 2003 at press
[15] Wahab Q, Hultman L, Willander M and Sundgren J E 1995 *J. Electron. Mater.* **24** 1345
[16] Wahab Q, Turan R, Hultman L, Willander M and Sundgren J-E 1996 *Thin Solid Films* **287** 252
[17] Johansson L I, Glans P-A, Wahab Q, Grehk T M, Eickhoff Th and Drube W 1999 *Appl. Surf. Sci.* **150** 137
[18] Virojanadara C, Glans P-A, Johansson L I, Eickhoff Th and Drube W 2001 *Appl. Surf. Sci.* **172** 253–9
[19] Mahowald P H, Friedman D J, Carey G P, Bertness K A and Yeah J J 1987 *J. Vac. Sci. Technol.* A **5** 2982
[20] Cumpson P J and Seah M P 1997 *Surf. Interface Anal.* **25** 430
[21] Virojanadara C and Johansson L I 2001 *Surf. Sci.* **472** L145
[22] Virojanadara C and Johansson L I 2002 *Surf. Sci.* **505** 358
[23] Johansson L I, Owman F and Mårtensson P 1996 *Phys. Rev.* B **53** 13793
[24] Muehlhoff L, Choyke W J, Bozack M J and Yates J T Jr 1986 *J. Appl. Phys.* **60** 2842
[25] Mårtensson P M, Owman F and Johansson L I 1997 *Phys. Status Solidi* b **202** 501
[26] Simon L, Kubler K, Ermolieff A and Billon T 1999 *Phys. Rev.* B **60** 5673
[27] Luth D-A, Miller T and Chiang T-C 1997 *Phys. Rev. Lett.* **79** 3014
[28] Amy F, Soukiassian P, Hwu Y-K and Brylinski C 1999 *Appl. Phys. Lett.* **75** 3360
[29] Amy F, Enriquez H, Soukiassian P, Storino P-F, Chabal Y J, Mayne A J, Dujardin G, Hwu Y K and Brylinski C 2001 *Phys. Rev. Lett.* **86** 4342
[30] Amy F, Soukiassian P, Hwu Y K and Brylinski C 2002 *Phys. Rev.* B **65** 165323
[31] Hoshino Y, Nishimura T, Yoneda T, Ogawa K, Namba H and Kido Y 2002 *Surf. Sci.* **505** 234
[32] Johansson L I, Virojanadara C, Eickhoff Th and Drube W 2003 *Surf. Sci.* **529** 515
[33] Johansson L I, Owman F and Mårtensson P 1996 *Surf. Sci.* **360** L484
[34] Browning R, Sobolewski M A and Helms C R 1998 *Phys. Rev.* B **38** 13407
[35] Pasquarello A, Hybertsen M S and Car R 1995 *Phys. Rev. Lett.* **74** 1024
[36] Eickhoff T and Drube W 2002 unpublished
[37] Virojanadara C and Johansson L I 2002 unpublished
[38] Virojanadara C and Johansson L I 2002 *Surf. Sci.* **519** 73
[39] Matsui F, Yeom H W, Amemiya K, Tono K and Ohta T 2000 *Phys. Rev. Lett.* **85** 630 and references therein
[40] Sakamoto K, Matsui F, Hirano M, Yeom H W, Zhang H M and Uhrberg R I G 2002 *Phys. Rev.* B **65** 201309
[41] Sakamoto K, Doi S, Ushima Y, Ohno K, Yeom H W, Ohta T, Suto S and Uchida W 1999 *Phys. Rev.* B **60** R8465
[42] Johansson L I, Glans P-A and Hellgren N 1998 *Surf. Sci.* **405** 288
[43] Yano H, Hirao T, Kimoto T and Matsunami H 2000 *Japan. J. Appl. Phys.* **39** 2008
[44] Kimoto T, Yamamoto T, Chen Zhi Ying, Yano H and Matsunami H 2001 *J. Appl. Phys.* **89** 6105
[45] Rauls E, Hajnal Z, Deak P and Frauenheim Th 2001 *Phys. Rev.* B **64** 245323